

The Role of Mechanical Properties and Structure of Type I Collagen Hydrogels on Colorectal Cancer Cell Migration

Hector Castro-Abril, Jónathan Heras, Jesús del Barrio, Laura Paz, Clara Alcaine, Marina Pérez Aliácar, Diego Garzón-Alvarado, Manuel Doblaré, and Ignacio Ochoa*

Mechanical interactions between cells and their microenvironment play an important role in determining cell fate, which is particularly relevant in metastasis, a process where cells invade tissue matrices with different mechanical properties. In vitro, type I collagen hydrogels have been commonly used for modeling the microenvironment due to its ubiquity in the human body. In this work, the combined influence of the stiffness of these hydrogels and their ultrastructure on the migration patterns of HCT-116 and HT-29 spheroids are analyzed. For this, six different types of pure type I collagen hydrogels by changing the collagen concentration and the gelation temperature are prepared. The stiffness of each sample is measured and its ultrastructure is characterized. Cell migration studies are then performed by seeding the spheroids in three different spatial conditions. It is shown that changes in the aforementioned parameters lead to differences in the mechanical stiffness of the matrices as well as the ultrastructure. These differences, in turn, lead to distinct cell migration patterns of HCT-116 and HT-29 spheroids in either of the spatial conditions tested. Based on these results, it is concluded that the stiffness and the ultrastructural organization of the matrix can actively modulate cell migration behavior in colorectal cancer spheroids.

major cause of cancer related deaths, accounting for up to 90% of the cases.^[1] In the past decades, it has been demonstrated that cell invasion and metastasis are events that do not depend exclusively on cells, but also on their interaction with the tumor microenvironment and its stromal components.^[2,3] Consequently, a plethora of either in vivo or in vitro approaches have been developed to study the migrating and invasive properties of cancer cells. In the case of the former, recently developed techniques, such as intravital microscopy (IVM), offer the possibility to visualize dynamic cell processes (such as cell invasion) in a living animal with a resolution comparable to that achieved in traditional cell cultures.^[4,5] However, this technique, as well as others that involve animal models, is expensive, hard to control, requires special equipment, and carries ethical issues due to the use of animals.^[5,6] Furthermore, tissue mechanical properties can vary among species and can be difficult to measure in vivo. In turn, in vitro studies are cheaper and easier to reproduce than

those in vivo, with the caveat that they fail to completely reproduce the complexity of a living organism. However, they provide powerful tools to comprehend the mechanobiological response

1. Introduction

Metastasis is the process whereby cancer cells successfully invade and colonize a foreign tissue. It has been reported as the

H. Castro-Abril, L. Paz, C. Alcaine, M. P. Aliácar, M. Doblaré, I. Ochoa
Tissue Microenvironment lab (TME lab)
Aragón Institute of Engineering Research (I3A)
University of Zaragoza
Zaragoza 50018, Spain
E-mail: iochgar@unizar.es

H. Castro-Abril, L. Paz, C. Alcaine, M. P. Aliácar, M. Doblaré, I. Ochoa
Instituto de Investigación Sanitaria Aragón (IISA)
Zaragoza 50018, Spain


H. Castro-Abril, D. Garzón-Alvarado
Biomimetics Lab
National University of Colombia
Bogotá 111321, Colombia

J. Heras
Grupo de Informática
University of La Rioja
La Rioja 26006, Spain

J. del Barrio
Instituto de Nanociencia y Materiales de Aragón (INMA)
Department of Organic Chemistry
CSIC-University of Zaragoza
Zaragoza 50018, Spain

L. Paz, M. P. Aliácar, M. Doblaré, I. Ochoa
Centro Investigación Biomédica en Red. Bioingeniería
Biomateriales y Nanomedicina (CIBER-BBN)
Zaragoza 50018, Spain

M. Doblaré, I. Ochoa
Nanjing Tech University
Nanjing 50018, China

 The ORCID identification number(s) for the author(s) of this article can be found under <https://doi.org/10.1002/mabi.202300108>

© 2023 The Authors. Macromolecular Bioscience published by Wiley-VCH GmbH. This is an open access article under the terms of the Creative Commons Attribution-NonCommercial License, which permits use, distribution and reproduction in any medium, provided the original work is properly cited and is not used for commercial purposes.

DOI: 10.1002/mabi.202300108

of different cells to changes in the stiffness of a substrate in both physiological and pathological scenarios, which has helped to elucidate the mechanisms by which cells migrate, proliferate, or differentiate in vivo.^[7–11] Early in vitro studies on migration and invasion have been conducted in scratch wound-healing assays.^[12] Yet, these platforms are limited since they fail to reproduce the 3D architecture of a living tissue and have a high degree of variability in their results.^[13,14] To circumvent these issues, 3D experiments have emerged in the past decades.^[15,16,25,26,17–24] The Boyden assay, an early example of these 3D experiments, is the benchmark technique to assess cancer cell invasion and migration.^[15] However, this approach has two main limitations. First, since it relies on external membranes to separate nonmigrating cells from those that migrated through such membranes, pore size of the membrane is a critical factor that directly impacts on the number of migrating cells.^[27] Additionally, since the membrane is made from artificial materials, the biological relevance of the migration results is limited.^[27,28] Second, it requires a chemical gradient to stimulate cell migration, which reduces the duration of the experiment due to the inherent difficulties in controlling the gradient resulting from the spatial configuration of the assay.^[13,28] Current strategies to study the invasion and migration patterns of cancer cells include the seeding of either single cells or aggregates (such as spheroids) in a hydrogel matrix, which can be made of alginate,^[29] matrigel,^[18] methacrylate gelatin (GelMa),^[30] poly(ethylene glycol)^[3,31] or solubilized type I collagen.^[17,22,23,32,33] From these, solubilized type I collagen is the most common material for preparing hydrogels. There are different reasons for this. First, collagen is a natural component of the great majority of tissues in a living organism, making it an excellent biocompatible material for generating scaffolds. Second, it is preferred over matrigel or comparable basal membrane-based matrices because metastatic events occur in the stromal layers of tissues, where type I collagen predominates. Alginate lacks the biomimetic characteristics of collagen-based hydrogels, despite the fact that it can be useful for different biomedical applications.^[34] Finally, contrary to GelMa, type I collagen hydrogels do not require external crosslinkers or catalysts that can potentially alter the biological response of cells. In the case of experiments involving type I collagen hydrogels and spheroids, samples can be mixed with an unpolymerized matrix solution and then deposited on top of a previously polymerized matrix layer or can also be suspended entirely inside a matrix without any underlying bed. From these strategies, cell migration can be potentially detected in every direction, as has been demonstrated by several studies.^[16–19,21–26] Nevertheless, information regarding the mechanical and ultrastructural characterization of the hydrogels, as well as their role in the observed results, is either absent or poorly reported, since these articles mainly focus on analyzing cell response to either biochemical signals or their interaction with other cell populations (usually from the tumor stroma). This is a major issue since it has been demonstrated, both in vivo and in vitro, that the mechanical environment affects the biological behavior of individual cells.^[35–38] In vitro studies have also demonstrated that the mechanical properties and the ultrastructure of different scaffolds, such as those made of type I collagen, can be modified by altering the final collagen content and the gelation temperature.^[39] For instance, Yang et al. reported that the mechanical properties of hydrogels polymerized following a

two-stage procedure (first left at 22 °C for a given amount of time and then transferred to 37 °C) were between those obtained for samples polymerized at constant temperatures of 22 °C and 37 °C.^[40] Similar results were obtained by Holder et al. despite using different polymerization temperatures and times.^[39] Finally, Seo et al.^[10] demonstrate that collagen fiber thickness and pore size can be controlled by adjusting the gelation temperature and that these parameters can lead to profound changes in the contractility and differentiation of adipose stromal cells (ASCs) into myofibroblasts.

Mechanical characterization of a material can be performed using different techniques depending on its nature and the aim of the research. In the case of type I collagen hydrogels, oscillatory rheometry is one of the most commonly used approaches to describe their overall mechanical behavior due to the fact that hydrogels, as well as most soft biological tissues, exhibit viscoelastic properties.^[3,41–43] This technique applies a fixed small amplitude sinusoidal deformation (with a prefixed frequency ω) to the hydrogel over a given time. From this measurement, the complex modulus $G^*(\omega) = G' + iG''$ can be determined, where G' and G'' are called the storage and loss moduli, respectively.^[44] The former is related to the strain energy stored during a deformation cycle and can be interpreted as the resistance of the hydrogel to deformation. Conversely, the latter is associated with the energy dissipated during the same cycle and can be interpreted as the resistance of the hydrogel to revert to its original configuration after deformation. Surface mechanical properties of a hydrogel can be determined by atomic force microscopy (AFM).^[45] This technique allows the characterization of the stiffness (expressed, for instance, in terms of the Young's modulus) of the surface of hydrogels under liquid physiological environments with nanometric resolution.^[45] This, combined with information of the fiber morphology obtained with scanning electron microscopy (SEM), provides valuable data about the mechanical landscape at the surface of a hydrogel.

This study aims to demonstrate how the localization of cell aggregates within type I collagen hydrogels and their polymerization processes, which alter their stiffness and fiber ultrastructure, can have a profound impact on the mechanobiological behavior of those aggregates. For this, we prepared type I collagen hydrogels with different collagen concentrations and polymerization schemes and characterized their mechanical properties by rheometry and AFM. We further analyzed the fiber morphology of the surface and inner zones of the samples by SEM. Then, we seeded HCT-116 and HT-29 spheroids at different locations on the hydrogels to study their migratory response and invasive capacity. Our results may contribute to the development of new therapeutic strategies based on the alteration of the mechanical properties of the surrounding uninvaded tumor stroma.

2. Results

2.1. Gelation Temperature Increases up to Two Orders of Magnitude the Overall Stiffness of a Hydrogel with a Fixed Concentration

With respect to the rheological behavior, **Figure 1** shows a comparative overview for a hydrogel with a final collagen concentration of 3.0 mg mL⁻¹ polymerized at 37 °C or following the

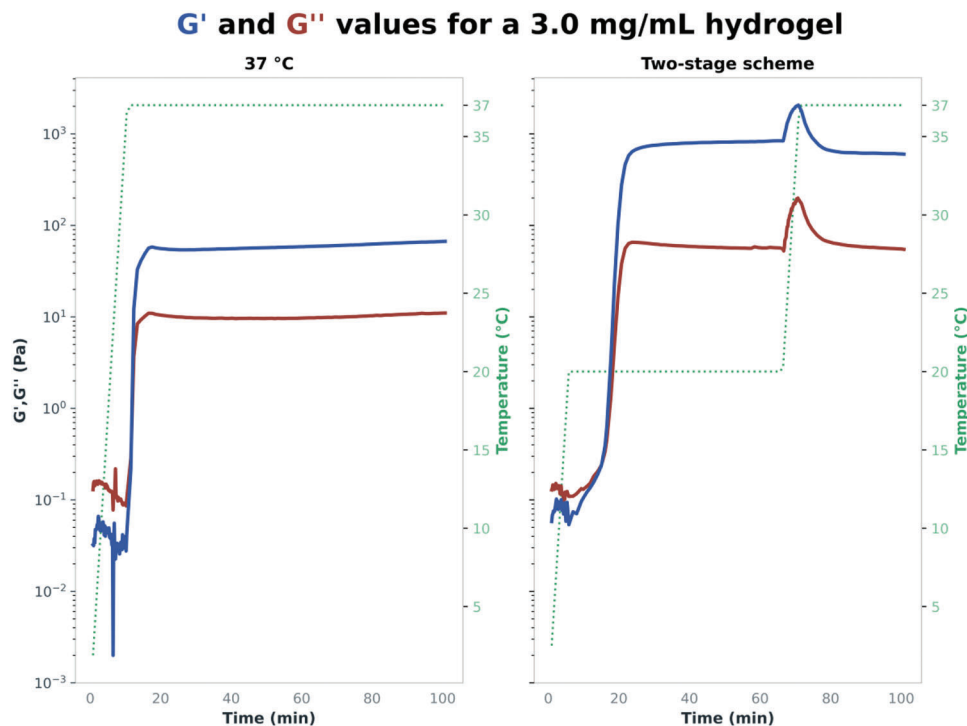


Figure 1. Rheological behavior of a hydrogel with a collagen concentration of 3.0 mg mL⁻¹. The hydrogel was either polymerized directly at 37 °C (left image of the Figure) or following the two-stage scheme (right image of the Figure). In both cases, the temperature scheme is represented by the green dotted line.

Table 1. Mechanical properties of the six types of hydrogels.

Concentration (mg mL ⁻¹)	Polymerization temperature	Rheological measurements of the hydrogels		AFM measurements of the hydrogels
		Mean storage modulus, G' [Pa]	Mean loss modulus, G'' [Pa]	Mean Young's modulus [Pa]
0.8	37 °C	1.7	1.2	161.6
0.8	Two-stage	107.5	9.4	310.1
1.5	37 °C	26.5	5.5	916.2
1.5	Two-stage	190.0	15.6	1123.0
3.0	37 °C	85.8	13.7	1230.0
3.0	Two stage	460	44.1	2026.0

two-stage scheme. Recalling the experimental procedures described in the previous section, in the cases where the hydrogels were polymerized at 37 °C, we placed the unpolymerized hydrogel solution inside a CO₂ incubator (with a constant temperature of 37 °C) for 30 min. In contrast, hydrogels polymerized following the two-stage scheme were deposited and left to polymerize at RT for 1 h before placing them inside the CO₂ incubator (with a constant temperature of 37 °C). For visualization purposes, only the first 100 min of the measurement are presented. In the samples polymerized at 37 °C, the moduli stabilized right after the gelation period ended. In those polymerized following the two-stage scheme, the values had a stable plateau that started after the gelation period and ended when the temperature was elevated to 37 °C. During this increase, both moduli suffered

a transient and unstable increase in their values. Interestingly, once the temperature reached 37 °C, their final values were very similar to those obtained prior to the temperature increase (from 20 to 37 °C). Regarding the other tested hydrogels, similar trends were obtained (Figures S1 and S2, Supporting Information), but with different values for $G'(\omega)$ and $G''(\omega)$. Values for the storage modulus (G') and loss modulus (G'') of all the tested hydrogels are given in Table 1.

When analyzing the values of G' (Table 1) under a fixed polymerization scheme, we observed that the stiffness of the hydrogels increased with the collagen concentration, despite the chosen gelation protocol. When the collagen concentration was fixed, we noticed that the temperature had a marked effect on the stiffness of the hydrogels. As seen in Table 1, the greatest values of

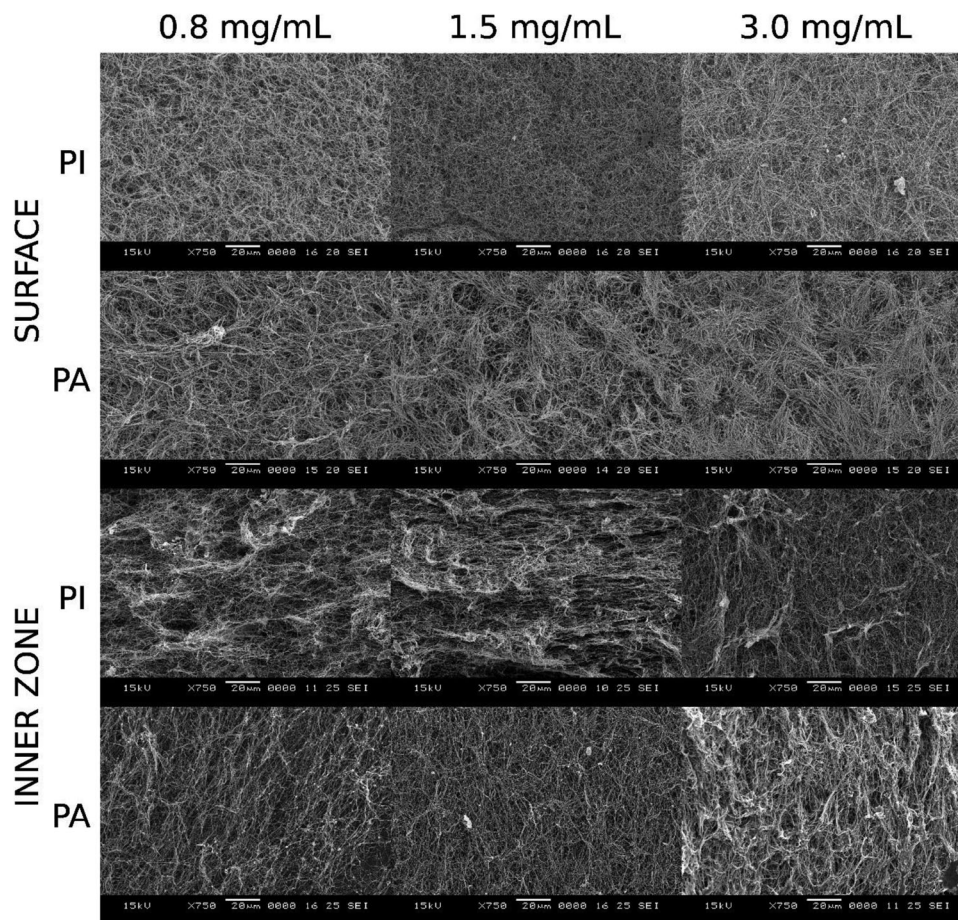


Figure 2. SEM images of the collagen fiber network present in the surface of the six tested hydrogels. Magnification: 750 \times .

both moduli were always obtained in the samples polymerized following the two-stage scheme. In addition, we observed that the storage ($G'(\omega)$) modulus for a hydrogel with a collagen concentration of 0.8 mg mL⁻¹ and polymerized following the two-stage scheme was approximately two orders of magnitude higher than the corresponding value for the same collagen concentration hydrogel polymerized at 37 °C. This trend was maintained for the rest of the tested concentrations. Nonetheless, the differences decreased as the collagen content increased. Thus, for hydrogels with a concentration of 1.5 mg mL⁻¹, the difference in magnitude was approximately seven-fold, whereas for those with a concentration of 3.0 mg mL⁻¹, the difference was approximately three fold.

2.2. Surface Stiffness of Hydrogels Is Modified by the Gelation Temperature

The mean Young's moduli for the different tested hydrogels are presented in Table 1. As expected, under a fixed polymerization temperature, collagen concentration significantly affected the stiffness of the hydrogels (p -value < 0.0001 for all cases). Indeed, hydrogels with low collagen concentration (0.8 mg mL⁻¹) had the lowest Young's moduli values (161.6 Pa for those poly-

merized at 37 °C and 310 Pa for those polymerized following the two-stage scheme), while those with the highest collagen content (3.0 mg mL⁻¹) had the greatest values (1230 Pa for the ones polymerized at 37 °C and 2026 Pa for the hydrogels polymerized following the two-stage scheme). For the hydrogels with intermediate concentration (1.5 mg mL⁻¹), Young's moduli values were in between the ones for the other concentrations (916 Pa for the polymerization at 37 °C and 1123 Pa for the two-stage scheme). In addition, under a fixed collagen concentration, the surfaces of hydrogels polymerized following the two-stage scheme were stiffer than those of samples polymerized directly at 37 °C.

2.3. Fiber Morphology Changes in Different Zones of a Hydrogel

2.3.1. Hydrogel Surface

The upper part of **Figure 2** shows representative images of the surface of the tested hydrogels at 750 magnifications. Qualitative evaluation of the morphology of the surface of the hydrogels revealed that the collagen fiber arrangement seemed to evolve from a loose and spider web-like layout, present in the 0.8 mg mL⁻¹ hydrogels, to a more organized and tight structure, with increasing fiber bundling in hydrogels with higher content of collagen,

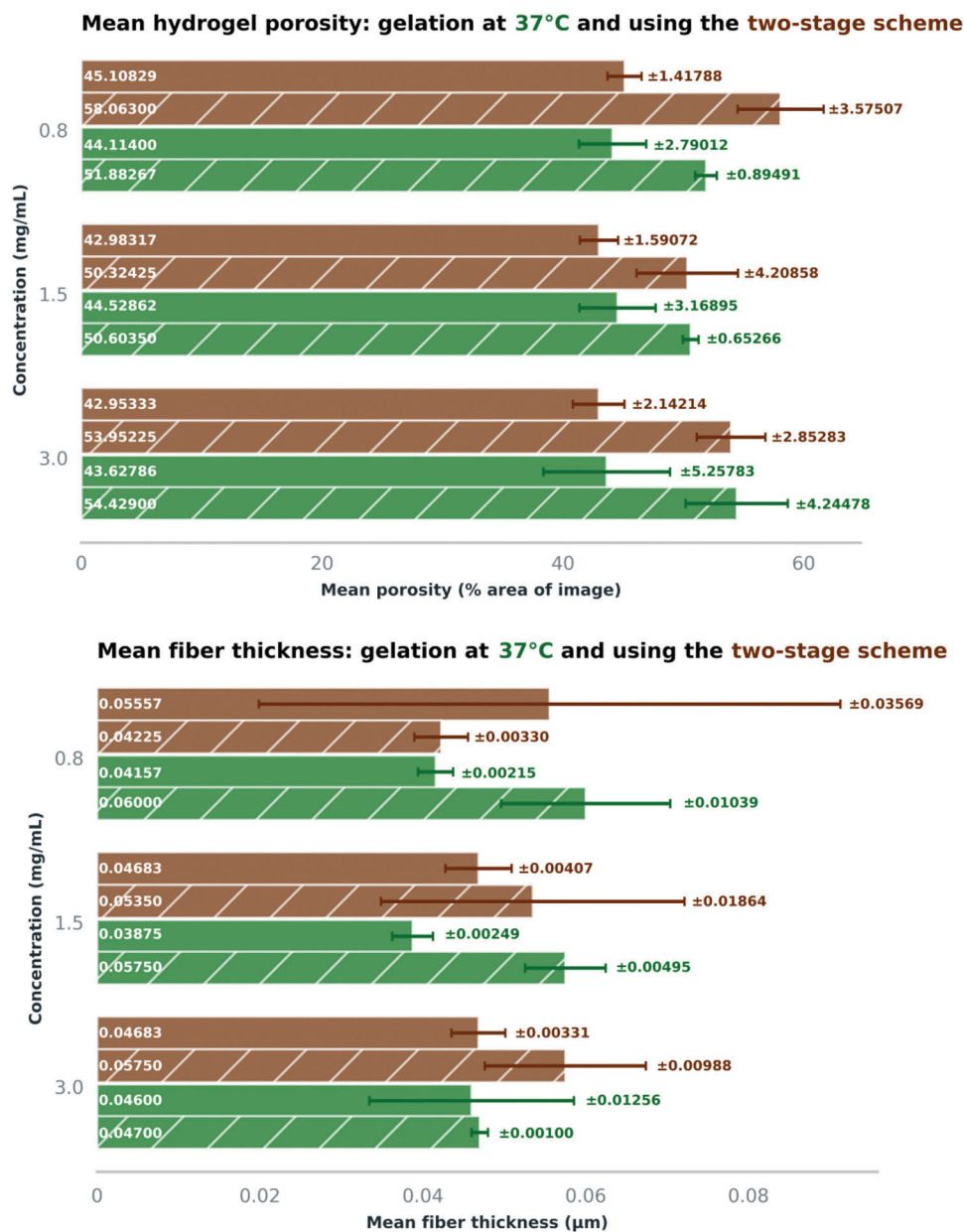


Figure 3. Quantitative analysis of the morphological structure of the collagen fiber network present in the different hydrogels. Solid bars indicate data from the surface of the hydrogels. Striped bars represent data from the inner surface of the samples.

such as that observed in the 1.5 and 3.0 mg mL⁻¹ samples. This behavior repeated in both polymerization schemes (directly at 37 °C or following the two-stage temperature), albeit with remarkable differences in the 3.0 mg mL⁻¹ hydrogel. Indeed, it was seen that fibers appeared more bundled in the two-stage temperature scheme than when polymerized directly at 37 °C.

2.3.2. Hydrogel Inner Structure

Representative images of the collagen distribution in the inner zones of the hydrogels are presented in the bottom part of Figure 2. As seen, fiber networks seemingly did not follow the

same trend as the one observed at the surface of the hydrogels when the collagen content was increased. However, in all images, fibers seemed to have a specific orientation. Regarding fiber thickness in the inner zones of the hydrogels (Figure 3), we observed that, in general, inner fibers were thicker than those at the surface of the hydrogels. This trend was also enhanced by the polymerization scheme. Indeed, the inner fibers of the samples polymerized at 37 °C (green striped bars in Figure 3) were also thicker than those of the hydrogels polymerized following the two-stage scheme (brown striped bars in Figure 3).

Results for quantitative analysis of fiber morphology for both the surface and inner zones of the hydrogels are presented in Figure 3. Data for the mean fiber thickness and porosity of the

hydrogels (\pm SD) for all the tested conditions measured at 750 \times magnifications are given as bar charts. With respect to the fiber thickness at the surface of the hydrogels (solid bars in Figure 3), we observed that, in both polymerization schemes, fibers seemed to decrease their thickness in the hydrogels with low (0.8 mg mL⁻¹) to intermediate (1.5 mg mL⁻¹) concentrations, which agrees with previous observations found in the literature.^[46] In addition, we found that the polymerization scheme also influences the thickness of the fibers. Indeed, hydrogels polymerized following the two-stage scheme (brown solid lines) had, in general, thicker fibers than those polymerized directly at 37 °C (green solid lines). In contrast, we noted that the hydrogels exhibited similar behavior in terms of porosity regardless of the chosen polymerization scheme. This suggests that the gelation temperature does not influence these parameters at the surface of a hydrogel.

2.3.3. HCT-116 and HT-29 Migration Patterns Are Modulated by a Combination of the Ultrastructure of the Hydrogels and Their Stiffness

Single Spheroids Seeded on Top of a Hydrogel (Unconstrained 2D Experiment)

Figure 4 (left part) shows the migration patterns of HCT-116 spheroids placed on top of previously polymerized hydrogels and surrounded by culture medium. In this experiment, cells migrated at the surface of the hydrogel in a predominantly collective fashion (with negligible cell clusters), regardless of the final collagen concentration or polymerization scheme. Furthermore, migration was not radially homogeneous but exhibited preferential directions, suggesting that the local distribution of the collagen fibers might promote these anisotropic migration patterns by increasing the local stiffness of the surface of the hydrogels. This was particularly evident in the cases in which the hydrogels were polymerized following the two-stage scheme. In turn, when HT-29 cells were seeded on top of a previously polymerized layer of hydrogel (left column of Figure 5), cell migration seemingly occurred in a combination of both collective and individual patterns. However, as in the case for HCT-116 spheroids, cells migrated in-plane and did not exhibit a radially homogeneous distribution.

Quantitative analyses of the HCT-116 mean spheroid and invaded areas (schematic representations of the measurements are depicted in Figure 6a) of the experiment described in this section are shown in Figure 7 and Table S1 (Supporting Information). According to our results, under a fixed collagen concentration, the polymerization scheme seemed to influence the size of the spheroids in a concentration-dependent manner, particularly for the low-concentration hydrogels (Table S7, Supporting Information). As such, for the spheroids seeded on top of hydrogels with a collagen concentration of 0.8 mg mL⁻¹, the percent differences in area were 23.9% (Table S1, Supporting Information) at the end of the experiment, followed by samples seeded on top of hydrogels of 1.5 mg mL⁻¹ (4.0%, Table S1, Supporting Information) and 3.0 mg mL⁻¹ (4.0%, Table S1, Supporting Information). For the other time points, we also found similar trends (Table S1, Supporting Information). In turn, within the same polymerization scheme, spheroids had a similar size in all

three tested concentrations (Table S8, Supporting Information). For the HT-29 spheroids, under a fixed collagen concentration of 3.0 mg mL⁻¹, the polymerization scheme did not have a significant influence on the spheroid size (Figure 8). Indeed, by the end of the experiment, the percent differences in area were approximately 4.6% (Table S2, Supporting Information), agreeing with the observed trend for the HCT-116 spheroids at the same concentration. However, in contrast to the HCT-116 cell line, HT-29 spheroids seeded on top of hydrogels polymerized at 37 °C were smaller than those seeded on top of hydrogels polymerized following the two-stage scheme (Table S17, Supporting Information).

As for the invaded area (orange lines in Figure 7), our results showed that the invaded area of HCT-116 spheroids increased with the collagen concentration (Table S9, Supporting Information). When the collagen concentration was fixed, cell invasion in the hydrogels polymerized at 37 °C was greater than that in the hydrogels polymerized following the two-stage scheme (Tables S1 and S10, Supporting Information). This was especially true for the hydrogels with low collagen concentration, where the percent differences were up to 15.2% by the end of the experiment. For the other concentrations, the percent difference in the invaded area decreased to 4.6% for the hydrogels of 1.5 mg mL⁻¹ and 1.2% for those with a concentration of 3.0 mg mL⁻¹ (Table S1, Supporting Information). In the case of HT-29 spheroids, under a fixed collagen concentration of 3.0 mg mL⁻¹, the invaded area was greater in the hydrogels polymerized following the two-stage scheme than in their counterpart at 37 °C (18.3%, Table S2, Supporting Information), which differed from the exhibited behavior of the HCT-116 spheroids seeded in the same condition. However, this increase was not statistically significant (Table S18, Supporting Information).

Lastly, regarding the spheroid to invaded area ratio, we observed that, despite the concentration or the polymerization scheme, the invaded area of HCT-116 spheroids was always greater than the spheroid area in all cases (Table S1, Supporting Information). This may be explained by the fact that spheroid cells are allowed to migrate freely along the surface of a hydrogel since they do not have mechanical constraints to restrict in-plane movement. In stark contrast, the invaded area by the HT-29 spheroid cells was smaller than the area of the spheroids.

Single Spheroids Seeded on Top of a Hydrogel, but Surrounded by Another Layer of Hydrogel (Constrained 2D Experiment): Figure 4 (central part) shows representative examples of the migration patterns in HCT-116 spheroids “sandwiched” inside the tested hydrogels. We noticed that cells migrated from the main mass and always remained at the interface between the two hydrogel layers in a radial pattern. In addition, an individual cell migration pattern was present in hydrogels with low (0.8 mg mL⁻¹) and intermediate (1.5 mg mL⁻¹) collagen concentrations. In both cases, individual cell clusters disseminated radially around the main tumor mass, increasing the occupied area inside the collagen matrix. This behavior started around the first day after seeding (Figure 6b and Figure S4, Supporting Information) and continued throughout the duration of the experiment, suggesting that in these concentrations, cells tended to migrate individually. Conversely, in hydrogels with high collagen concentrations (3.0 mg mL⁻¹), there was no cell spreading around the spheroids, leaving a well-encapsulated tumor mass throughout the duration of the

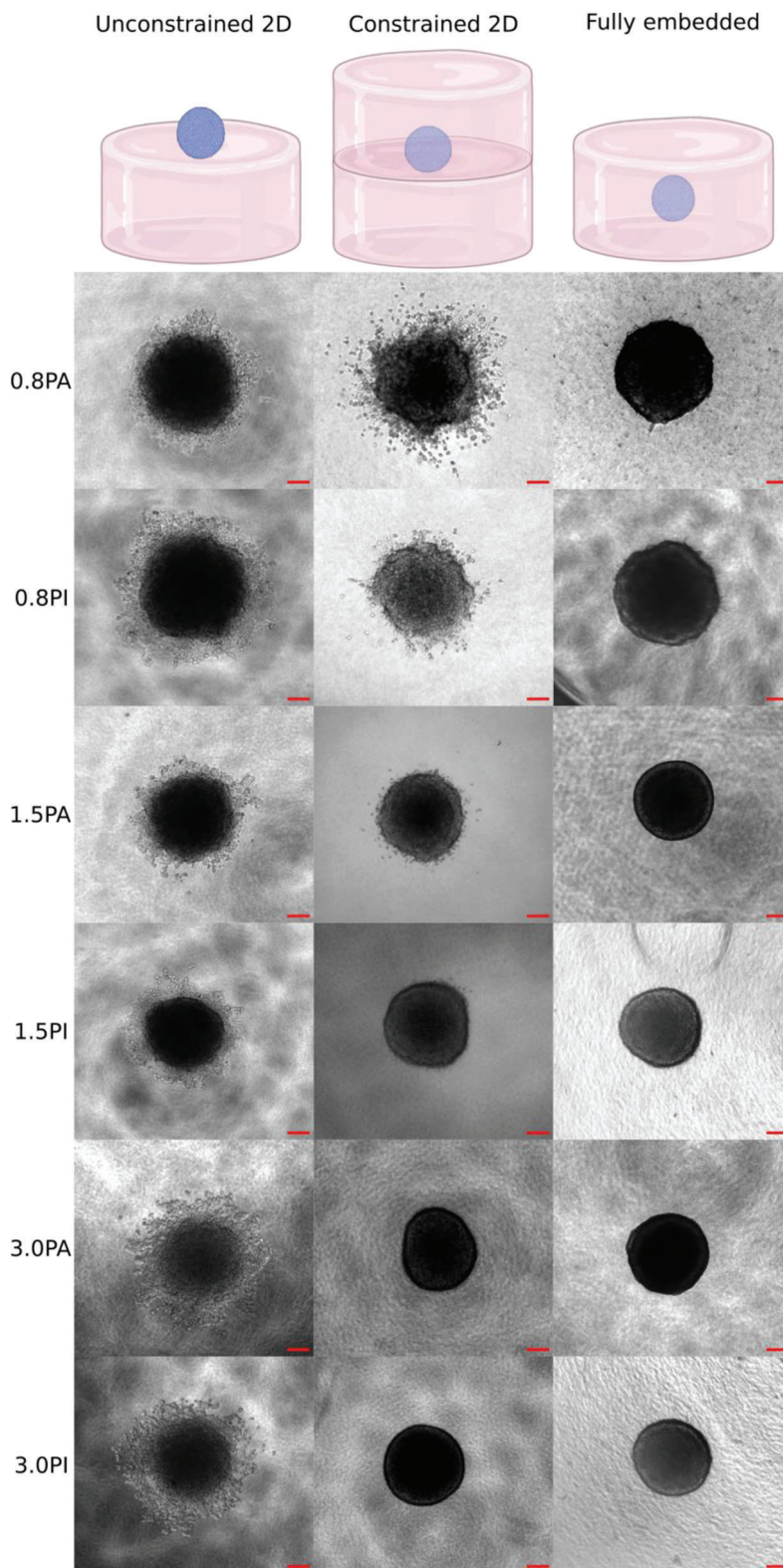


Figure 4. Migration patterns obtained for HCT-116 spheroids in the Unconstrained 2D (left panel of the Figure), Constrained 2D (center panel of the Figure), and fully embedded (right panel of the Figure) experiments. The time at which the images were taken was 72 h after the start of the experiments. The top panel depicts graphic representations of the mentioned cell-related experiments (created with biorender). Scale bar: 100 μm . PA: polymerization following the two-stage scheme. PI: polymerization at 37 $^{\circ}\text{C}$.

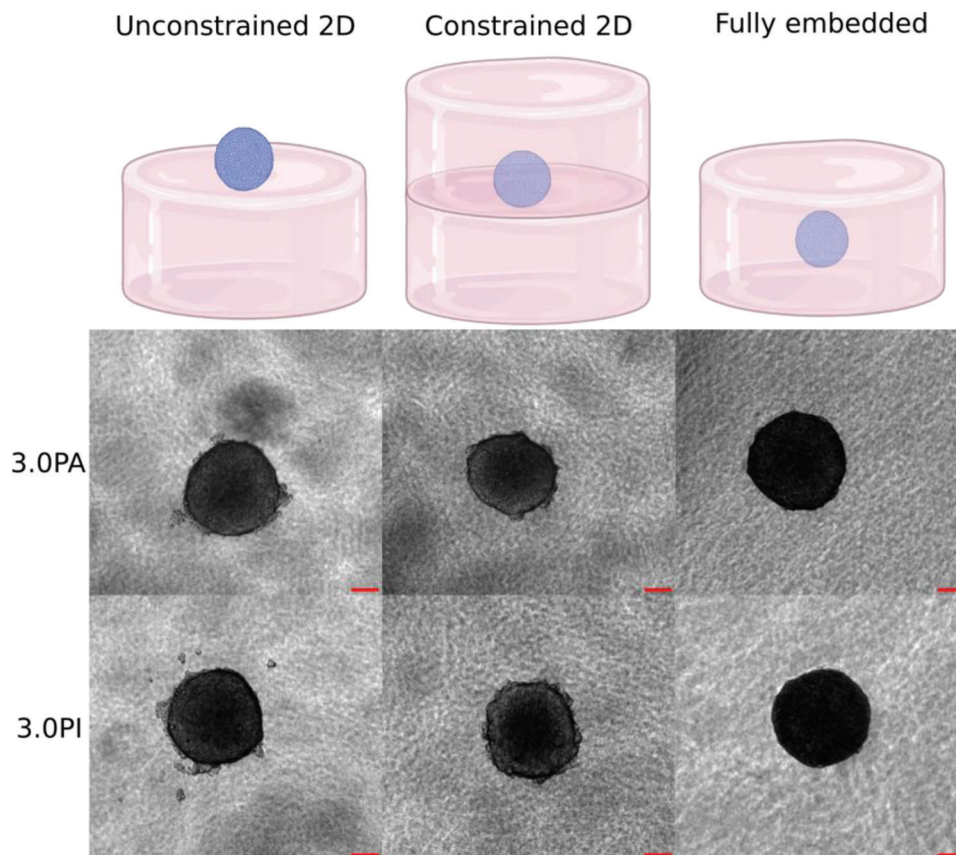


Figure 5. Migration patterns obtained for HT-29 spheroids in the Unconstrained 2D (left panel of the Figure), Constrained 2D (center panel of the Figure), and fully embedded (right panel of the Figure) experiments. The time at which the images were taken was 72 h after the start of the experiments. The top panel depicts graphic representations of the mentioned cell-related experiments (created with biorender). Scale bar: 100 μm . PA: polymerization following the two-stage scheme. PI: polymerization at 37 $^{\circ}\text{C}$.

experiment. For the HT-29 spheroids (Figure 5 and Figure S7, Supporting Information), cells migrated in a predominantly collective fashion in either of the polymerization schemes used. This behavior contrasted with the HCT-116 spheroids under the same collagen concentration (3.0 mg mL^{-1}).

Regarding the HCT-116 mean spheroid area (blue lines in Figure 9), we observed that, as in the unconstrained experiment, it was also dependent on the collagen concentration and the polymerization scheme. Indeed, in hydrogels polymerized following the two-stage scheme, spheroids decreased in area as the collagen content increased and had the opposite behavior in samples polymerized at 37 $^{\circ}\text{C}$ (Table S11, Supporting Information). Instead, when the concentration was fixed and the polymerization scheme was changed, the spheroid area had variable behavior. For hydrogels with low and intermediate collagen concentrations (respectively, 0.8 and 1.5 mg mL^{-1}), spheroids “sandwiched” between layers polymerized at 37 $^{\circ}\text{C}$ were smaller than the ones in between hydrogels polymerized following the two-stage scheme (see Tables S3 and S12, Supporting Information). In contrast, spheroids between hydrogels of high collagen concentration (3.0 mg mL^{-1}) and polymerized at 37 $^{\circ}\text{C}$ were bigger, although not statistically significant (Tables S3 and S12, Supporting Information). Nevertheless, despite this heterogeneity, the differences in area decreased with the collagen concentration,

as in the previously described unconstrained experiment. When analyzing the effects of the polymerization scheme on the HT-29 spheroids with a fixed collagen concentration of 3.0 mg mL^{-1} (blue lines in Figure 10), we noticed that, similarly to the case of the HCT-116 cell line, spheroids seeded between two layers of hydrogels polymerized at 37 $^{\circ}\text{C}$ were smaller than their counterparts polymerized following the two-stage scheme, with a percent difference of approximately 7.7% by the end of the experiment (Table S4, Supporting Information), albeit with no statistical relevance (Table S19, Supporting Information).

With respect to the invaded area of HCT-116 cells (orange lines in Figure 9), we found that, under a fixed polymerization scheme, the invaded area decreased as the collagen content in the hydrogels increased (Table S13, Supporting Information). When the collagen concentration was fixed, the biggest differences were found in the low concentration (0.8 mg mL^{-1}) hydrogels (Tables S3 and S14, Supporting Information). In fact, at every time point (starting at 24 h), the percent differences revealed that the spheroids “sandwiched” in hydrogels polymerized following the two-stage scheme invaded an area at least 100% larger than their counterparts in the hydrogels polymerized directly at 37 $^{\circ}\text{C}$ (Table S3, Supporting Information). This phenomenon was also present, albeit on a smaller scale, in the intermediate concentration (1.5 mg mL^{-1}) hydrogels (Table S3, Supporting In-

Temporal evolution of spheroid and invaded area in:

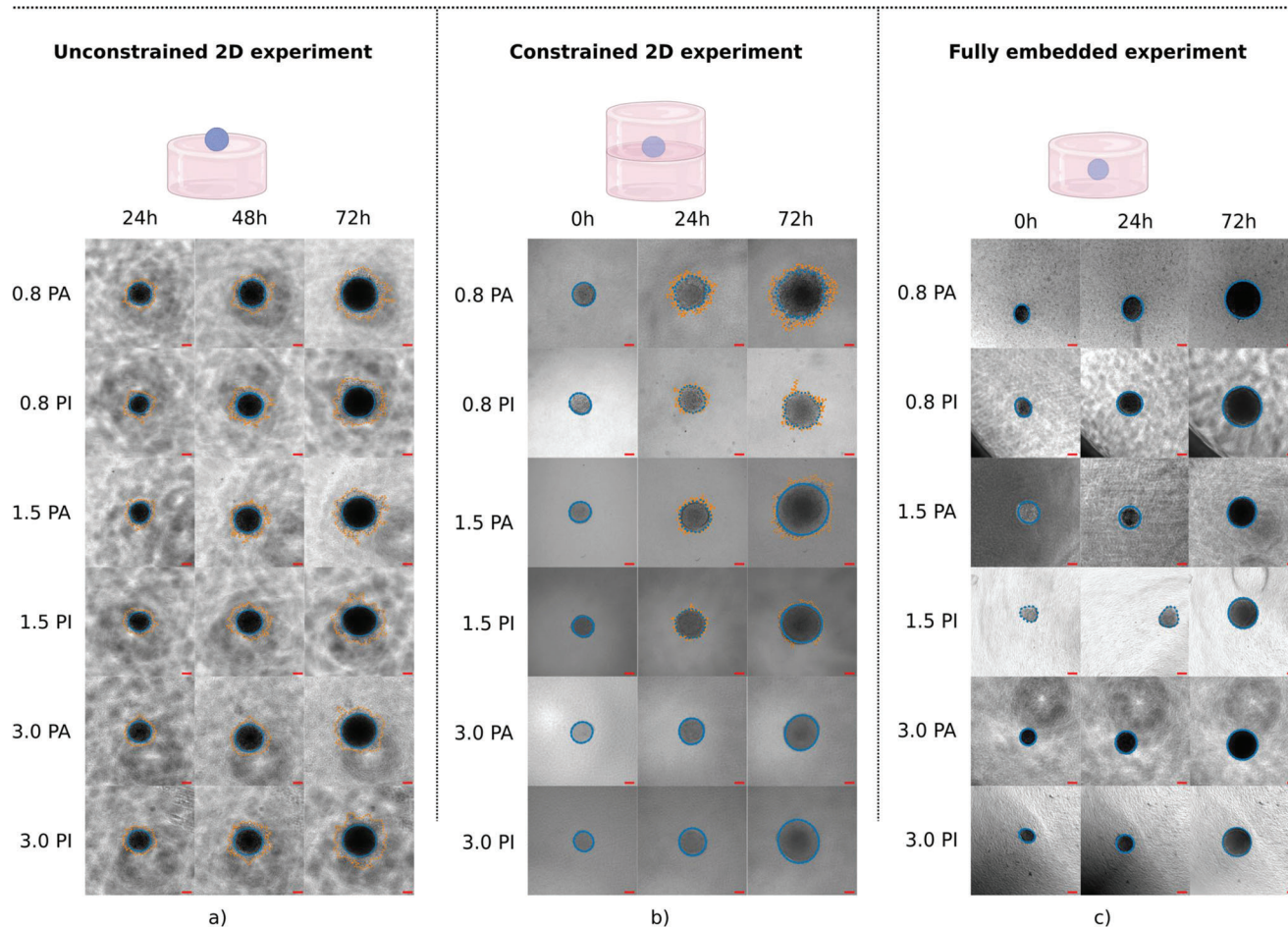


Figure 6. Cell migration measurements for HCT-116 spheroids seeded according to the experiments defined in Methods. a) Cell migration patterns in the unconstrained 2D experiment. b) Cell migration patterns in the constrained 2D experiment. c) Cell migration patterns in the fully embedded experiment. In all cases, the spheroid area is highlighted in blue, whereas the invaded area is depicted in orange. The top panel depicts graphic representations of the mentioned cell-related experiments (created with biorender). PA: Polymerization following the two-stage scheme. PI: Polymerization at 37 °C. Scale bar: 100 μm .

formation). In contrast, for the spheroids “sandwiched” between hydrogels of high collagen concentration (3.0 mg mL^{-1}), there were no differences in the invaded area since, as we described above, cells did not migrate from the spheroids in either of the polymerization schemes. For the HT-29 spheroids (orange lines in Figure 10), the invaded area was larger in the cases where the hydrogels were polymerized at 37 °C (Table S4, Supporting Information). Furthermore, this result was also significant, as seen in Table S20 (Supporting Information).

Last, the values observed in the percent differences in the HCT-116 spheroid to invaded area ratio (last two columns in Table S3, Supporting Information) as well as for the HT-29 spheroids (last two columns in Table S4, Supporting Information) indicated that the area occupied by the invading cells was smaller compared to the spheroid size.

Single Spheroids Embedded inside a Hydrogel (Fully Embedded Experiment): Figure 4 (right part) shows representative examples of the temporal evolution of the spheroids fully suspended

inside the tested hydrogels. In all cases, there were no cells migrating from the main mass at the end of the experiment. This trend was maintained throughout the duration of the experiment (Figure 6c).

Concerning the HCT-116 spheroid area (blue lines in Figure 11), we observed that, under a fixed polymerization scheme, spheroids tended to decrease in area as the collagen concentration in the hydrogels increased (Table S15, Supporting Information). However, for the cases of spheroids embedded in hydrogels polymerized following the two-stage scheme, the results were not statistically significant (Table S15, Supporting Information). In turn, when the collagen concentration was fixed, the spheroids embedded inside hydrogels polymerized at 37 °C were bigger than their counterparts embedded in hydrogels polymerized following the two-stage scheme (see Tables S5 and S16, Supporting Information). By the end of the experiment, the largest percent differences (21.9%) were again present in the hydrogels with low collagen concentration (0.8 mg

Temporal spheroid and invaded area changes for the tested hydrogels

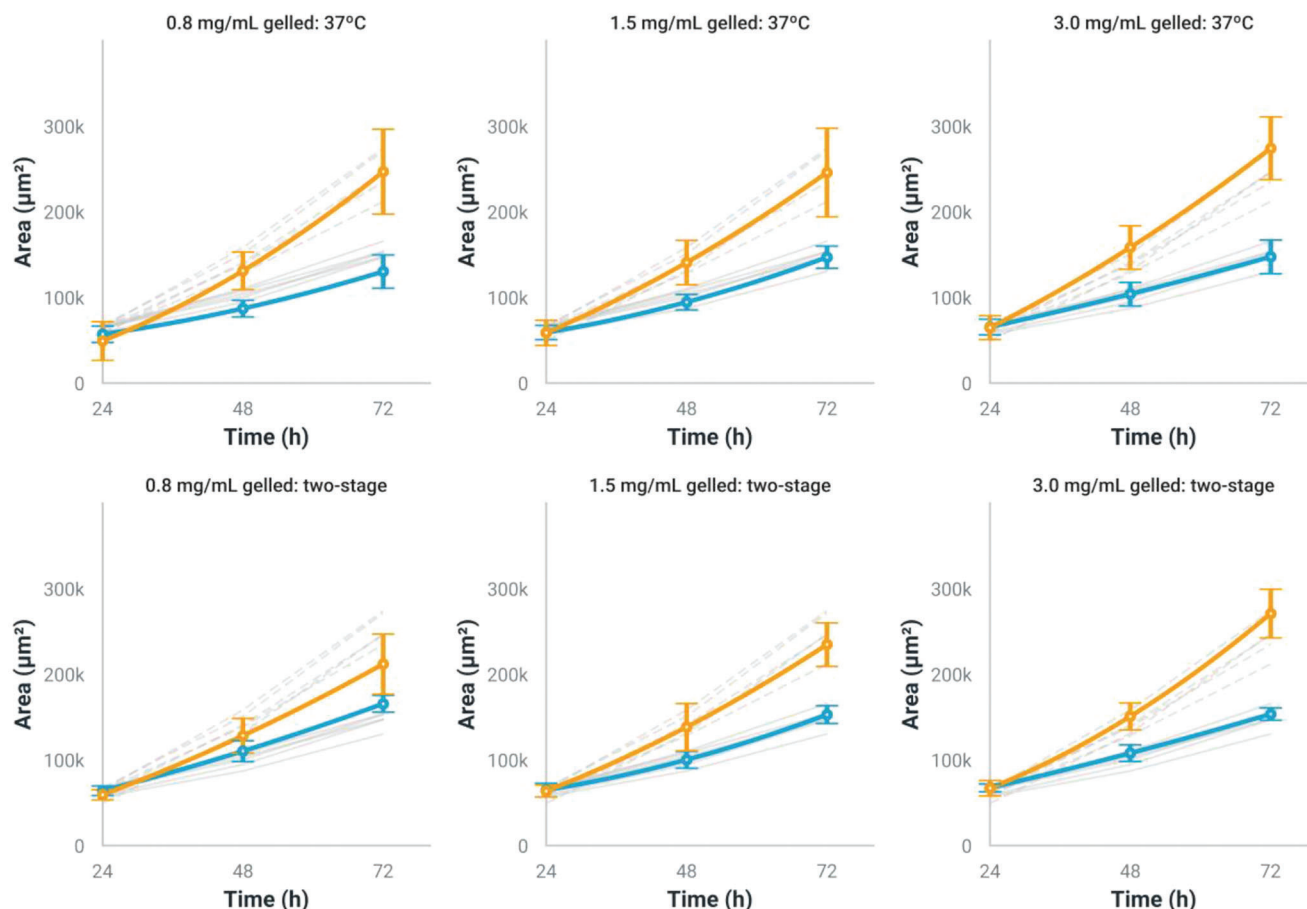


Figure 7. Time evolution of HCT-116 spheroid and invaded area growth of the unconstrained 2D experiment. Time scale: hours. Area scale: μm^2 . Continuous lines: Spheroid areas. Dashed lines: invaded areas. The gray color (in both solid and continuous lines) represents either the spheroid or invaded area evolution for the rest of the 5 non highlighted experiments.

mL^{-1}), followed by those with a concentration of 3.0 mg mL^{-1} (10.9%), and, finally, those with a concentration of 1.5 mg mL^{-1} (9.8%). In contrast, for the HT-29 spheroids (Figure 12 and Table S6, Supporting Information), the spheroids embedded inside hydrogels polymerized at 37°C were smaller than their counterparts embedded in hydrogels polymerized following the two-stage scheme by approximately 11.4% at the end of the experiment. Nevertheless, the differences in area were not statistically relevant (Table S21, Supporting Information).

Finally, the lack of invading cells in either HCT-116 or HT-29 spheroids (orange lines in Figures 11 and 12) in any of the tested scenarios suggests that the increased pore size and porosity of the inner zones of the hydrogels, compared to the surface of the hydrogels, prevents cell migration of the HCT cells.

3. Discussion

In the last decade, in vitro studies have demonstrated the importance of mechanical interactions between cells and their surrounding microenvironment in understanding cancer progres-

sion. However, most of these studies undermine the importance of the effect of the fabrication parameters of the scaffolds (usually made of type I collagen hydrogels) on the mechanobiological response of cells. In this study, we used pure type I collagen hydrogels fabricated with different concentrations and polymerization procedures as a model to understand the influence of their mechanical properties (measured by rheometry and AFM) and ultrastructural organization (measured by SEM) on the migration patterns of HCT-116 cells organized in multicellular spheroids.

We have observed that both storage and loss moduli increased and stabilized once the gelation period finished, similar to previous studies.^[40,46–48] In addition, the value of the storage modulus of the polymerized hydrogels, regardless of the polymerization procedure, increased at higher collagen concentrations. This behavior has been reported before and has been attributed to the content of the protein,^[41,48–50] since the increasing collagen concentration in the hydrogels results in a rise of available fibers that form a denser and, therefore, stiffer network. Furthermore, the values of the storage and loss moduli (Table 1) after polymerization at 37°C were of the same order of magnitude as those

Temporal spheroid and invaded area changes for the tested hydrogels

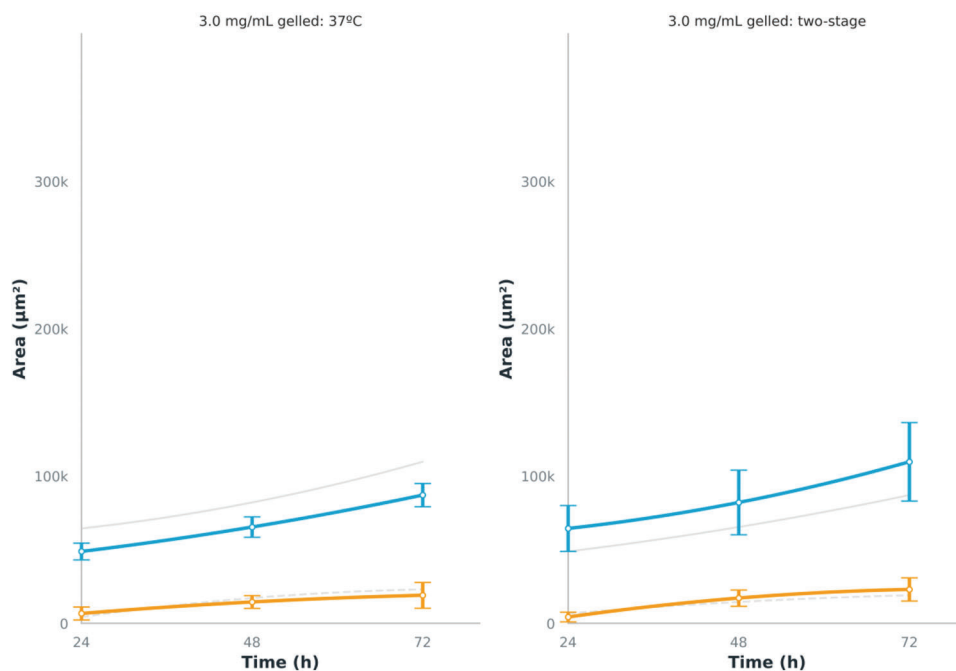


Figure 8. Time evolution of HCT-116 spheroid and invaded area growth of the unconstrained 2D experiment. Time scale: hours. Area scale: μm^2 . Continuous lines: Spheroid areas. Dashed lines: invaded areas. The gray color (in both solid and continuous lines) represents either the spheroid or invaded area evolution for the rest of the 5 non highlighted experiments.

of other hydrogels with analogous collagen contents.^[41–43,51] For instance, Yang et al.^[41] reported that the storage modulus of a 1.5 mg mL^{-1} hydrogel polymerized at 37°C was approximately 13.14 Pa , whereas the reported value herein (for the same collagen concentration and polymerization temperature) was approximately 28 Pa . Piechocka et al.^[43] using type I collagen with telopeptides reported a G' value for hydrogels with a collagen concentration of 3.0 mg mL^{-1} (polymerized at 37°C) of nearly 100 Pa , whereas the G' value reported in this document for this hydrogel and polymerization temperature was approximately 103 Pa . Last, Yang et al.^[40] show the rheological behavior of a 4.0 mg mL^{-1} hydrogel polymerized following a two-stage temperature scheme similar to the one used in this manuscript, with a stable G' value lower than the obtained value for a collagen of 3.0 mg mL^{-1} here but in the same order of magnitude.

In turn, the effect of the polymerization temperature on the moduli values, with a fixed collagen concentration, indicates that the temperature at which the hydrogels initiate their polymerization is critical for their final stiffness, as described.^[39] Indeed, high polymerization temperatures accelerate the formation of the collagen fiber network, yielding less organized structures with small pore sizes that ultimately alter the mechanical properties of the samples.^[40,49] In our case, samples subjected to an initial annealing at 20°C for 1 h followed by a second annealing at 37°C (total annealing time was 24 h) reached higher storage and loss moduli values than those directly annealed at 37°C .

With respect to the surface Young's modulus (Table 1), our results may also be explained in a similar manner to the rheological behavior. Indeed, the number of fibers present at the surface is also expected to increase with the collagen concentration,

thus raising the surface stiffness of hydrogels. In addition, as discussed in the above paragraph, the effect of the polymerization scheme on the surface stiffness of the hydrogels is related to the fiber network formation kinetics.^[40] Thus, we anticipated that the stiffness of the surface of the hydrogels polymerized following the two-stage scheme would be higher than its counterpart in samples polymerized directly at 37°C . Lastly, results of the surface stiffness are within the range of experimental measurements performed by Brauchle et al.^[11] on collagen-rich zones of both healthy colon and carcinoma tissues. The authors report a mean Young's modulus ranging from 0.9 to 4.4 KPa for colon carcinomas and a range of 0.5 to 1.0 KPa for healthy tissue. Data for our hydrogels are within an approximate range of 0.2 to 2.0 KPa (Table 1), which, according to results from the authors, are closer to healthy tissue. Our results also agree with those obtained by Pamplona et al. regarding the stiffness of healthy colon tissue.^[52] However, contrary to those authors, we did not require to prepare a GelMA hydrogel to obtain stiffness similar to those of healthy tissue.

Comparison of the SEM data at the surface and inner zones of the hydrogels (Figure 3) showed that collagen fibers were thicker at the inner zones of all hydrogels than at their surface. This phenomenon suggests that inner fibers act as weight-bearing columns that support the collagenous surface while maintaining the 3D architecture of the hydrogels. Changes in collagen fiber thickness depending on the location within the tissue have been previously reported in vivo by Ushiki et al.^[53] In their research, the authors found that collagen fibers were thicker in the outer zones of peripheral nerves (epineurium) than in their inner zones (endoneurium). These findings highlight the relationship

Temporal spheroid and invaded area changes for the tested hydrogels

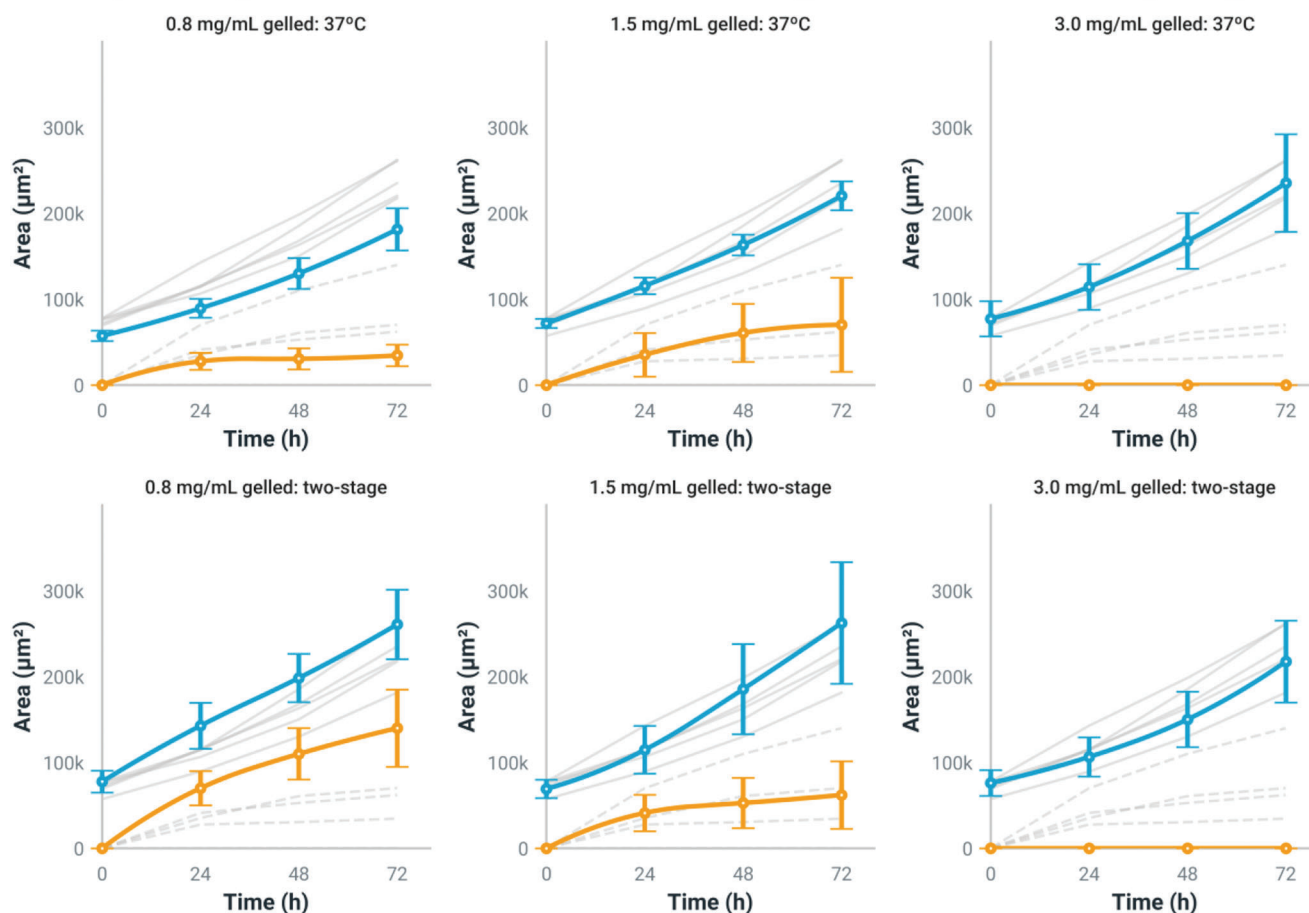


Figure 9. Time evolution of HCT-116 spheroid and invaded area growth for the constrained 2D experiment. Time scale: hours. Area scale: μm^2 . Continuous lines: Spheroid areas. Dashed lines: invaded areas. The gray color (in both solid and continuous lines) represents either the spheroid or invaded area evolution for the rest of the 5 non highlighted experiments.

between the function of the fiber within the tissue and its location. Indeed, in the case of the nerves, the thicker collagen fibers serve as a protective agent against tensile forces, whereas in the hydrogels, they serve as a support column, as explained above. Furthermore, the thickness of the fibers at the inner zones of the hydrogels (Figure 3) had similar values to those reported in previous reports.^[46,48,50,54] Regarding the observed fiber orientation at the inner zones of the hydrogels, we believe this is likely an artifact generated by the cut performed to visualize the interior of the hydrogels. Lastly, the differences in the fiber distribution at the surface of the hydrogels (as a function of collagen concentration) agree with previous findings in literature, which state that collagen ultrastructure can be modulated with the polymerization temperature.^[40,46] Therefore, the results for this section corroborate that the polymerization temperature has a direct impact on the fiber distribution at the surface of the hydrogels,^[49] which, in turn, would explain the variability in the stiffness of the surface.

Concerning cell-related experiments, the heterogeneity of the results suggests that the contribution of the stiffness and ultrastructure of the hydrogels to the migration patterns varies depending on the location of the spheroid in the hydrogel. Thus,

for the unconstrained 2D experiment, (Figures 7 and 8 and Figures S3 and S6, Supporting Information) the local stiffness of the surface of the hydrogels may be the predominant factor in determining the invaded area. Indeed, an increasingly stiff surface, as in the case for HCT-116 and HT-29 spheroids, stimulates the detachment of cells from the tumor mass and their subsequent invasion of the surrounding tissue (Figures 4, 5, and 6a), possibly by stimulating the focal adhesion-clusters and cytoskeletal contractility of cells.^[38,55] This observation agrees with previous findings.^[56] On the contrary, for the experiments where the spheroid was mixed with an unpolymerized hydrogel solution and then seeded on top of a previously polymerized layer of hydrogel (Figures 4, 5, and 6b, and Figures S4 and S7, Supporting Information), the predominant factor seems to be the overall stiffness of the layer surrounding the spheroid. In fact, despite the previously polymerized layer of hydrogel, which, as we stated above, provides an attractive surface for cell migration, the presence of an additional surrounding layer of hydrogel (that polymerizes with the spheroid inside) generates a new constraint that hinders cell movement, a result that agrees with the trends observed by Liu et al.^[16] This constraint is directly related to the

Temporal spheroid and invaded area changes for the tested hydrogels

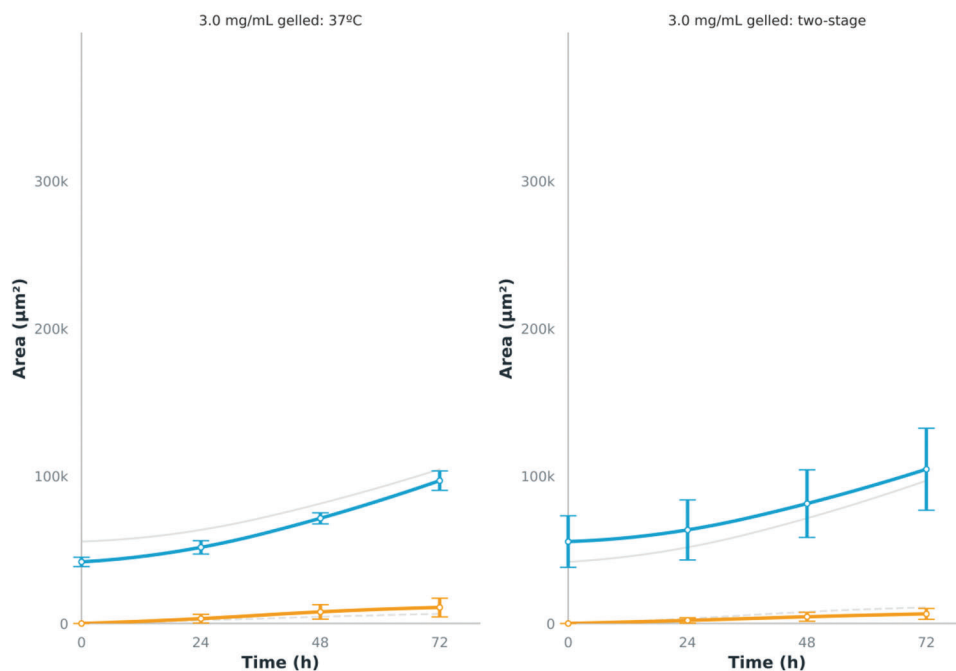


Figure 10. Time evolution of HT-29 spheroid and invaded area growth for the constrained 2D experiment. Time scale: hours. Area scale: μm^2 . Continuous lines: Spheroid areas. Dashed lines: invaded areas. The gray color (in both solid and continuous lines) represents either the spheroid or invaded area evolution for the rest of the 5 non highlighted experiments.

stiffness of the hydrogel as well as the fiber bundling when the collagen concentration is increased. As a case in point, for samples with a collagen concentration of 3.0 mg mL^{-1} , the constraint generated by the layer of hydrogel surrounding the hydrogel is powerful enough to prevent cell migration in the HCT-116 spheroids and reduce the invaded area in the HT-29 spheroids (Figures 4 and 5). Recently, Mao et al. developed an experimental model to study the role of the mechanics of interfacial microenvironments in the migration of cancer cells.^[57] Although the authors perform their study on functionalized PDMS surfaces, a key difference from our study, they do highlight the importance of the stiffness of the interface in cell migration. This agrees with our observations, especially for the constrained 2D experiment. Nevertheless, the observed in-plane migration for the unconstrained and constrained 2D experiments may be explained by the orientation of the fibers at the surface of the hydrogels. Indeed, at the surface of the hydrogels, fiber network collapses forming a planar surface that ultimately favors cell migration along the plane.^[58] Finally, the complete absence of cell migration seen in the fully embedded experiments (Figures 4, 5, 6c, and Figures S5 and S8, Supporting Information), which agrees with the results shown by Dolznig et al.^[17] and Ilina et al.^[9] may be mainly explained by the fact that, in the absence of planar surfaces inside the hydrogels, the forces exerted by the cells on the surrounding matrix may not be strong enough to promote cell detachment from the aggregates, either as a single entity or a multicellular body.^[35,36] This may be related to the thickness of the fibers, as has been demonstrated by Mukherjee et al.^[59] Indeed, thin fibers do not provide an adequate surface area to promote cell spreading and the creation of adhesion points, result-

ing in impeded cell movement.^[59] Furthermore, pore size may also influence the lack of cell migration in the fully embedded experiments, since it has been shown that this parameter also influences cell migration within a given matrix.^[60]

On the other hand, the migration patterns shown in Figures 4 and 5 seem to be primarily regulated by the boundary restrictions imposed on the spheroids. Therefore, in the unconstrained 2D experiment, where a single collagen surface is in contact with the spheroid, HCT-116 cells migrate preferentially in a collective manner (Figure 4), which is a crucial characteristic of epithelial cells.^[35,38] In the case of the HT-29 spheroids, cells seem to migrate preferentially as small clusters that primarily remain close to the tumor mass (Figure S6, Supporting Information). However, the conjoint proliferation of these clusters and their proximity to the main mass results in the seemingly hybrid migratory patterns (cell sheets and clusters) observed in Figure 5. By contrast, in the constrained 2D experiment, HCT-116 cells are forced to change their migration patterns (from collective to individual), likely because they have to overcome the physical barrier imposed by the surrounding hydrogel.^[38] This observation also holds true for the HT-29 cells (Figure 5), since cells also shifted their migrating mode (from individual to collective). On the contrary, in the hydrogels with a final collagen concentration of 3.0 mg mL^{-1} (the last two rows of the middle column in Figure 4), HT-29 cells were able to invade their immediate vicinity (in a collective manner) despite the mechanical barrier imposed by such a matrix. However, the invaded area was very small compared to the size of the spheroid (Table S4, Supporting Information). Recently, Ilina et al.^[9] observed uniform migration patterns for MCF-7 breast cancer spheroids at the interface between a plastic surface and

Temporal spheroid and invaded area changes for the tested hydrogels

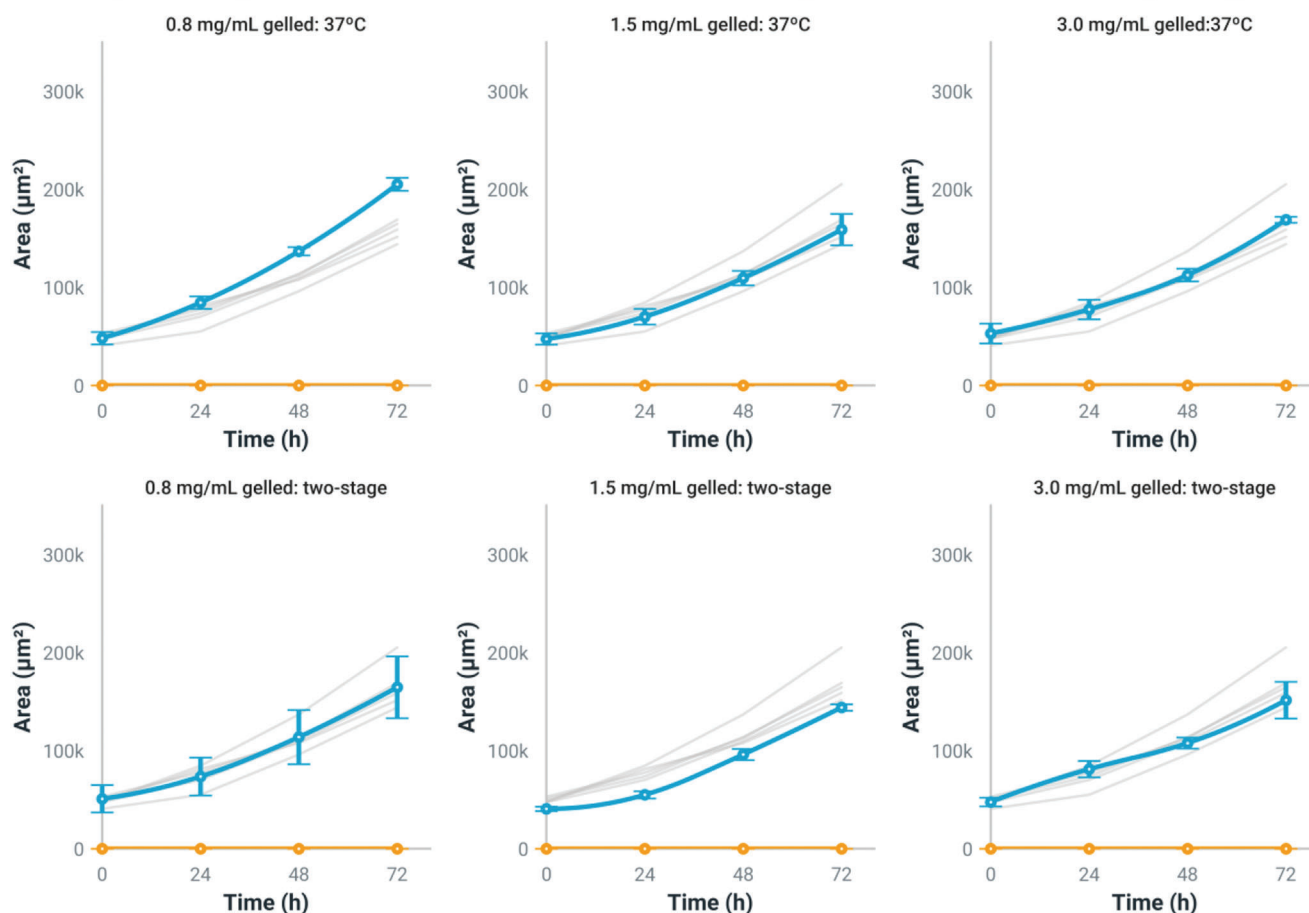


Figure 11. Time evolution of HCT-116 spheroid and invaded area growth of the fully embedded experiment. Time scale: hours. Area scale: μm^2 . The gray color represents the spheroid area evolution for the rest of the 5 non highlighted experiments.

the collagen matrix, with cells migrating on the plastic surface. In our results, migration occurred at the interface of the collagen matrices and was not uniform, and the invaded area was not as large as that of MCF-7 spheroids. These dissimilarities in the invaded area may be explained by the fact that a plastic surface has a higher stiffness and a more organized structure than a collagen surface.

In terms of the directionality of migrating cells, the observed anisotropy in the direction of migrating cells, especially for the HCT-116 spheroids in the unconstrained 2D experiment, may be explained by a combination of the variability in the local fiber thickness and orientation. Indeed, these two parameters may explain the presence of the sharp planar invasion fronts seen in Figure 4 despite the radially distributed cell sheets surrounding the spheroids, since it has been demonstrated that fiber thickness may alter the directionality and persistence of single cells.^[55] Altogether, these findings highlight the importance of fiber morphology and distribution in the hydrogels for the migrating potential of colorectal cancer cells and are in accordance with previous studies.^[61,62] Thus, the uninvaded biophysical microenvironment surrounding the tumor, expressed in terms of the stiff-

ness and ultrastructure of the surrounding collagen fibers, may become a potential target for new therapeutic strategies.

Despite the evidence presented in this document regarding the modulating role of hydrogel mechanics on cell migration, there are several limitations that must be considered. First, during rheological measurements, we did not completely reproduce the environmental conditions of the hydrogels, especially those involved in cell experiments. For instance, we measured the rheological properties of the hydrogels in the absence of CO_2 . However, cell-related experiments had the gas present. The presence of CO_2 may impact the overall mechanical stiffness since it is employed to maintain a physiological pH of 7.4 for appropriate cell culture. This is an important issue because pH is a known regulating factor of the mechanical properties of a hydrogel.^[49] Nevertheless, we have explored this issue by adding HEPES buffer to the hydrogel solution. This substance is commonly used in cell culture since it maintains a stable physiological pH in environments devoid of CO_2 . After adding this compound to the hydrogel solution and performing the rheology, we found that there were not significant differences between the moduli values (results not shown). In second place, the model only contemplates a single protein as the component of the hydrogels. This

Temporal spheroid and invaded area changes for the tested hydrogels

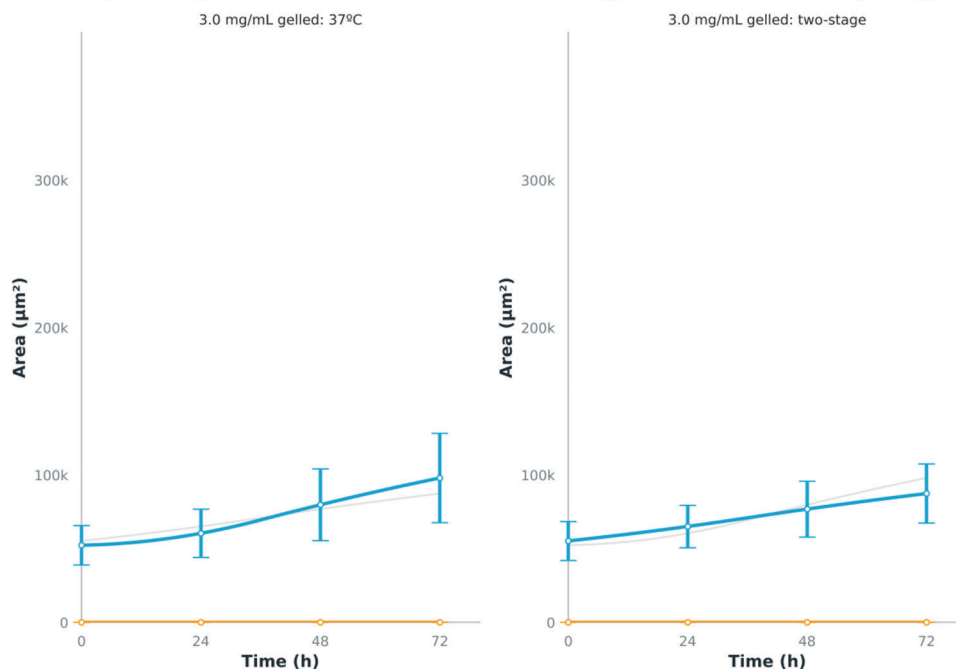


Figure 12. Time evolution of HT-29 spheroid and invaded area growth of the fully embedded experiment. Time scale: hours. Area scale: μm^2 . The gray color represents the spheroid area evolution for the rest of the 5 non highlighted experiments.

also needs to be taken into consideration, since in vivo matrices are not only comprised of type I collagen, and the presence of other molecules may also impact the migration pattern of cells. In third place, we have performed our studies in a relatively small spectrum of collagen concentrations (0.8, 1.5, and 3.0 mg mL^{-1}). Although the stiffness of our hydrogels was comparable to that of collagen-rich zones of healthy colon tissue,^[11] future studies in hydrogels with higher concentrations should be conducted to evaluate spheroid cell migration in cancer-associated microenvironments. Another important factor that was not taken into consideration in this manuscript is related to the effect of matrix remodeling. As has been stated by Brauchle et al., colon cancer cells actively remodel their surrounding matrix in order to generate stiffer and more attractive pathways to facilitate the invasion of healthy tissue.^[11] Finally, in this model, we did not apply external signals, such as chemoattractant gradients, to stimulate cell migration. The presence of external signaling is also important for cell migration, since it has been demonstrated that in both physiological and pathological scenarios, such as cancer, cells can be forced to migrate from their original location towards new zones due to these external signals.

4. Conclusions

In conclusion, we have demonstrated that variations in both the hydrogels stiffness and the ultrastructural organization of the fibers, caused by the polymerization temperature and the collagen concentration of the hydrogels, lead to profound changes in the migration capacity as well as the migration patterns of HCT-116 or HT-29 spheroid cells. This observation highlights the relevance of the fabrication parameters of the hydrogels on

the mechanobiological response of cells and may serve as a guiding tool for future research.

5. Experimental Section

Cell Culture: Human colon carcinoma HCT-116 and HT-29 cell lines were purchased from the American Type Culture Collection and routinely maintained in high glucose Dulbecco's modified Eagle medium (DMEM, 4.5 g L^{-1} glucose, Biowest, ID number: MS01HO1001) supplemented with 10% v/v fetal bovine serum (FBS, Gibco, Lot number: 2307592, non-USA origin), 1% v/v L-glutamine (Gibco, Reference number: A12860-01) and 1% v/v penicillin/streptomycin (Lonza, Lot number: 21E195302). Cell cultures were kept inside a TEB-1000 humidified incubator (EBERS Medical Technology) at 37°C , 5% CO_2 , and 95% air.

Stable Cell Transfection with EGFP: HCT-116 cells were stably transfected with EGFP using lentiviral vectors, which were kindly provided by Dr. Prats from the University Paul Sabatier in Toulouse, France. Briefly, approximately 5×10^4 cells were seeded in each well of a 24-well plate and incubated in a TEB-1000 humidified incubator (EBERS Medical Technology) at 37°C , 5% CO_2 , and 95% air for 24 h to allow cell attachment. Then, growth medium was removed, and cells were washed twice with 1x PBS (HyClone, Lot number: AH30017338). A mixture of the lentivirus and Protamine-supplemented OptiMEM ($5 \mu\text{g mL}^{-1}$, Sigma-Aldrich, P4020) at a 1:1 ratio was added to the cells and left for 24 h. Thereafter, the transfection medium was replaced with growth medium, and cells were separately maintained for two more weeks before use to ensure the complete removal of viral particles. Transfection efficiency was checked by fluorescence microscopy and flow cytometry (BD, FACSAria). More than 90% of the cells were found to be EGFP-positive.

Spheroid Generation: Homotypic HCT-116 or HT-29 spheroids were generated using the hanging drop method and a mixture of cell suspension supplemented with methylcellulose. Briefly, methylcellulose stock solution was first prepared by dissolving 6 g of high viscosity methylcellulose (Sigma, M052) in 500 mL of high glucose Dulbecco's modified Eagle medium (DMEM, 4.5 g L^{-1} glucose, Biowest, ID number: MS01HO1001).

Then, cells were trypsinized with trypsin EDTA (Corning, Lot number: 02822006), counted, and the suspension of cells was mixed with the methylcellulose stock solution at a 4:1 ratio. Last, 25 μL droplets (with a cell concentration of 1000 cells per droplet) were placed on the inner surface of a Petri dish lid. The Petri dish was then filled with sterile water to prevent evaporation of the droplets and placed inside an incubator at 37 °C and 5% CO₂ for 48 h. This time frame ensured a single, well-defined spheroid was formed inside each droplet. The initial cell number was approximately 1000 cells per spheroid.

Hydrogel Preparation: 3D culture experiments were performed using rat tail type I collagen hydrogels (Corning, Reference: 10224442) placed inside a 96-flat bottom plate. Hydrogels were prepared according to a previous protocol [32] in three final collagen concentrations (0.8, 1.5, and 3.0 mg mL⁻¹). Preparation and deposition of the collagen hydrogels were performed at 0 °C to prevent premature polymerization of the solution. In addition, the plates and the mixing vessels were also placed and kept at 0 °C.

Hydrogels Polymerization: Once deposited in the wells, the hydrogels were polymerized following two different schemes. In the first one, samples were placed inside a CO₂ incubator at a constant temperature of 37 °C for 30 min. In the second scheme, named the two-stage scheme, hydrogel solutions were polymerized at RT (20 °C inside the laminar flow cabinet) for 1 h and then placed at 37 °C inside the incubator. In either case, following polymerization, 100 μL of growth medium was added at the top of the polymerized hydrogels, and the plates were placed back inside the CO₂ incubator.

In summary, the experiments consisted of polymerizing three different collagen hydrogels (with final concentrations of 0.8, 1.5, and 3.0 mg mL⁻¹) in two different temperature schemes (either following the two-stage scheme or directly at 37 °C), resulting in six different types of samples.

Hydrogel Rheological Measurements: The rheological characterization of the hydrogels, in the absence of cells, was performed on a Haake Mars 40 rheometer with a parallel plate-plate geometry (gap size 1 mm, plate diameter 25 mm). Briefly, the samples were prepared at 0 °C as described in the previous section and transferred to the lower plate, which was pre-cooled to 0 °C, and the upper geometry was lowered to evenly distribute the solution of the sample and confine it. A thin layer of a low-viscosity silicon oil was then applied to the edge of the sample to prevent evaporation. In some cases, the temperature of the sample was raised from 0 to 37 °C, and then it was kept constant at 37 °C for the remainder of the measurement. In some other cases, the temperature was raised from 0 to 20 °C and kept constant at 20 °C for 1 h. Afterward, it was raised again to 37 °C and kept constant for the rest of the test. Each sample was monitored at constant shearing amplitude and frequency (0.1 Hz) for a period of 24 h to ensure sample equilibration. All time sweeps were performed within the linear viscoelastic regime. After the equilibration period, an amplitude sweep was recorded at a constant frequency and a constant temperature of 37 °C. Each rheological measurement was performed on at least three independent samples.

Mechanical Characterization of the Hydrogel Surface: To evaluate the stiffness of the surface of the tested hydrogels, the Young's modulus of the gel surface was measured with an atomic force microscope (AFM) Nanowizard 3 system (JPK Instruments, Germany) mounted on an optical inverted microscope (Nikon-Eclipse). For each gel condition, small drops of 30 μL were polymerized in a Petri dish (TPP Techno Plastic Products AG, 93040) and covered with DMEM medium (DMEM, Biowest, ID number: MS01HO1001). The Petri dish was placed on the PetriDishHeater (JPK Instruments, Germany) stage to maintain a constant temperature of 37 °C. AFM measurements were performed in liquid with qBioAC probes (NanoANdMore GMBH) treated with anti-adherence rinsing solution (Stemcell, Lot number: 07010) to minimize gel adhesion during cantilever retraction. Tip CB3 was chosen due to the adequacy of its nominal spring constant (0.06 N m⁻¹) for samples on the Pa scale. The experimental spring constant of each used tip was determined by the Thermal Noise Method.^[63] The calibrated cantilever was positioned over a gel drop, and force-spectroscopy measurements were performed in the AFM contact mode at high Z-lengths (5 μm) and slow speeds (2 $\mu\text{m s}^{-1}$). At least

100 force-spectroscopy curves were acquired for each gelling condition. Force spectroscopy curves were then processed with DP Software (JPK Instruments, Germany) and fitted to a Hertz model modified for paraboloid indentors (JPK Instruments, 2008) to obtain the Young's moduli.

Imaging of the Collagen Fiber Network and Fibril Structure in the Hydrogels: For the surface characterization of the collagen fiber network, a new set of hydrogels was prepared according to the protocol described above. After polymerization, the samples were fixed in glutaraldehyde (2.5% v/v) for 30 min at RT. Afterward, they were washed with PBS and stored at 4 °C overnight. Next, hydrogels were dehydrated in an ascending ethanol series up to 100% and dried for 3 h using a critical point dryer (Leica EM CPD300). After this step, samples were coated with gold/palladium nanoparticles and examined by SEM (JEOL JSM 6360-LV) operated at 15 kV acceleration voltage. Images of two different zones of the surface of the hydrogels were taken at 750 and 2000 magnifications. In turn, for the characterization of the inner structure of the hydrogel network, the samples used for analyzing the surface network were fractured and coated again with the same nanoparticles, and the fractured zones were examined by SEM. In both cases, at least three samples per condition were prepared, and three zones per sample were imaged.

Invasion and Migration Patterns of Colorectal Cancer HCT-116 and HT-29 Cell Lines under Different Mechanical Environments: In order to analyze the invasion and migration patterns of the HCT-116 and HT-29 cells in aggregated (spheroid) arrangements in the defined hydrogels, the following sets of experiments were performed: 1) single spheroids seeded on top of the hydrogel (unconstrained 2D experiment); 2) single spheroids seeded on top of the hydrogel but surrounded by another layer of hydrogel (constrained 2D experiment); and 3) single spheroids fully embedded inside the hydrogel (fully embedded experiment). HCT-116 spheroids were seeded in all six types of hydrogels (described above), whereas HT-29 spheroids were seeded in samples with the highest collagen concentration. Pictures were taken daily for 3 days using a Leica DMI8 Thunder. In each of the aforementioned experiments, two main parameters were measured: the size of the spheroids and the invasion fronts. The spheroid size corresponded to the area of the spheroid mass. In turn, the invaded area corresponded to the migrating cells that stemmed from the spheroids. In addition to these main parameters, the percentage difference of the achieved spheroid size between the two polymerization schemes within a fixed collagen concentration ($\Delta_{x_i^t, C, x_j^t, C}$) at each timepoint was also calculated as follows:

$$\Delta_{x_i^t, C, x_j^t, C} = \frac{2(x_i^t, C - x_j^t, C)}{x_i^t, C + x_j^t, C} \quad (1)$$

where x_i^t, C is the mean spheroid size at time t , for the polymerization scheme i , under a fixed concentration C . With these values, the resulting average of the spheroid size percentage difference for the three concentrations at every time point was obtained. In all these calculations, the sub-index i represents a polymerization occurring directly at 37 °C, whereas the sub-index j represents the two-stage polymerization scheme.

In a similar fashion, the percentage differences for the invaded area and the spheroid size to invaded area ratio were also calculated. In the following sections, the experiments mentioned above will be briefly described. All experiments were performed in at least two independent replicates (10 or more samples per replicate).

Single Spheroids Seeded on Top of a Hydrogel (Unconstrained 2D Experiment): A volume of 60 μL per well of unpolymerized hydrogel solution with a fixed concentration was deposited into the wells of a 96-well plate and left to polymerize according to the chosen gelation temperature scheme. Then, single spheroids consisting of approximately 1000 initial cells were suspended in growth medium and seeded on top of these polymerized hydrogels. For each well with hydrogel, a single spheroid was seeded. Afterward, the plates were placed in the CO₂ incubator.

Single Spheroids Seeded on Top of a Hydrogel but Surrounded by Another Layer of Hydrogel (Constrained 2D Experiment): Like the previous experiment, a first layer of collagen hydrogel (volume of 60 μL) with a fixed collagen concentration was deposited and polymerized inside a 96-well plate with a flat bottom following a chosen gelation temperature scheme. Once this layer was polymerized, 50 μL of a mixture containing a single spheroid (1000 initial cells) and collagen hydrogel solution (with the same collagen concentration as that of the first layer of hydrogel) was deposited on top of the first layer and allowed to polymerize following the same gelation scheme as the first layer. After the polymerization of this new layer, 100 μL of growth medium was added to maintain the culture.

Single Spheroids Fully Embedded Inside a Hydrogel (Fully Embedded Experiment): In this experiment, a volume of unpolymerized hydrogel solution (100 μL) was deposited inside a 96-well plate with a flat bottom. Immediately following this procedure, single spheroids (1000 initial cells) were seeded inside the solution. Afterwards, the plate was continuously flipped upside down during the gelation process to ensure that the spheroids did not attach to the plastic of the plates.

Image Analysis: Analysis of the fiber structure in both confocal reflectance and SEM images was also performed. For SEM images, pore-related parameters (mean size and the percentage of the image “occupied” by the pores, which is here denoted as “porosity”) and fiber-related parameters (mean length and mean thickness) were measured at 750 magnifications. All measurements are reported as mean \pm standard deviation. Regarding the experiments involving spheroids, changes in the area of the spheroids and the invaded area stemming from the spheroids were measured using a custom plugin developed in Fiji (<http://fiji.sc/Fiji>). More details regarding the algorithm can be found in the paper published by Lacalle et al.^[64]

Statistical Analysis: Statistical analyses were performed in R (version 4.2.0).^[65] Data related to the temporal evolution of multicellular spheroids were analyzed with linear mixed models^[66] by using the lme function of the nlme package.^[67] In these models, time was set as the independent variable and the area (either of the spheroid or the one corresponding to the invasion) was set as the dependent variable. In addition, the collagen concentration in the hydrogels and the polymerization schemes were defined as the moderator variables. Furthermore, the models included up to the quadratic terms of the time variable as well as their interactions with other variables. Lastly, random intercepts for the samples (spheroids) and random slopes for time were also included in the models. The inclusion of both parameters (random slopes and random intercepts) accounts for the variability in spheroid growth as well as in their initial area and allows a better fit of the data.^[68] Results with a p -value under 0.05 were considered statistically relevant, whereas those with a p -value greater than 0.05 were considered nonsignificant.

Supporting Information

Supporting Information is available from the Wiley Online Library or from the author.

Acknowledgements

This work was supported by the European Union’s Moore4Medical project under grant numbers G.A. n° 876190 and PCI2020-112064, and the Republic of Colombia’s Ministry of Science (Minciencias) “Convocatoria 785 de Doctorados Nacionales” programme. The experimental tests have been performed by the ICTS “NANBIOSIS”, more specifically by the Tissue & Scaffold Characterization Unit (U13) of the CIBER in Bioengineering, Biomaterials, and Nanomedicine (CIBER-BBN) at the University of Zaragoza. The authors acknowledge the use of “Servicio General de Apoyo a la Investigación-SAI, Universidad de Zaragoza” for their support in the preparation and imaging of SEM photographs of the hydrogels.

Conflict of Interest

The authors declare no conflict of interest.

Data Availability Statement

The data that support the findings of this study are available from the corresponding author upon reasonable request.

Keywords

collagen, colorectal cancer, hydrogels, invasion, migration

Received: April 13, 2023

Revised: May 5, 2023

Published online:

- [1] P. S. Steeg, *Nat. Med.* **2006**, *12*, 895.
- [2] S. Cattin, L. Ramont, C. Rüegg, *Front. Bioeng. Biotechnol.* **2018**, <https://doi.org/10.3389/fbioe.2018.00097>.
- [3] G. Ciccone, O. Dobre, G. M. Gibson, J. M. Rey, C. Gonzalez-Garcia, M. Vassalli, M. Salmeron-Sanchez, M. Tassieri, *Adv. Healthcare Mater.* **2020**, *9*, 2000517.
- [4] R. Weigert, M. Sramkova, L. Parente, P. Amornphimoltham, A. Masedunskas, *Histochem. Cell Biol.* **2010**, *133*, 481.
- [5] Y. W. Choo, J. Jeong, K. Jung, *BMB Rep.* **2020**, *53*, 357.
- [6] N. Levy, *Int. J. Stroke* **2012**, *7*, 440.
- [7] P. P. Provenzano, D. R. Inman, K. W. Eliceiri, J. G. Knittel, L. Yan, C. T. Rueden, J. G. White, P. J. Keely, *BMC Med.* **2008**, *6*, 11.
- [8] M. Mak, F. Spill, R. D. Kamm, M. H. Zaman, *J. Biomech. Eng.* **2016**, *138*, 21004.
- [9] O. Iliina, P. G. Gritsenko, S. Syga, J. Lippoldt, C. A. M. La Porta, O. Chepizhko, S. Grosser, M. Vullings, G.-J. Bakker, J. Staruß, P. Bult, S. Zapperi, J. A. Käs, A. Deutsch, P. Friedl, *Nat. Cell Biol.* **2020**, *22*, 1103.
- [10] B. o. R. i. Seo, X. Chen, L. u. Ling, Y. H. Song, A. A. Shimpi, S. Choi, J. Gonzalez, J. Sapudom, K. Wang, R. C. Andresen Eguiluz, D. Gourdon, V. B. Shenoy, C. Fischbach, *Proc. Natl. Acad. Sci. USA* **2020**, *117*, 11387.
- [11] E. Brauchle, J. Kasper, R. Daum, N. Schierbaum, C. Falch, A. Kirschniak, T. E. Schäffer, K. Schenke-Layland, *Matrix Biol.* **2018**, *68-69*, 180.
- [12] L. G. Rodriguez, X. Wu, J.-L. Guan, *Methods Mol. Biol.* **2005**, *294*, 23.
- [13] K. F. Lei, H.-P. Tseng, C.-Y. i. Lee, N.-M. Tsang, *Sci. Rep.* **2016**, *6*, 25557.
- [14] N. Kramer, A. Walzl, C. Unger, M. Rosner, G. Krupitza, M. Hengstschläger, H. Dolznig, *Mutat. Res. - Rev. Mutat. Res.* **2013**, *752*, 10.
- [15] H.-C. Chen, *Methods Mol. Biol.* **2005**, *294*, 15.
- [16] H. Liu, T. Lu, G.-J. Kremers, A. L. B. Seynhaeve, T. L. M. Ten Hagen, *Biol. Proced. Online* **2020**, *22*, 3.
- [17] H. Dolznig, C. Rupp, C. Puri, C. Haslinger, N. Schweifer, E. Wieser, D. Kerjaschki, P. Garin-Chesa, *Am. J. Pathol.* **2011**, *179*, 487.
- [18] C. J. Olsen, J. Moreira, E. M. Lukanidin, N. S. Ambartsumian, *BMC Cancer* **2010**, *10*, 444.
- [19] J.-I. l. Park, J. Lee, J.-u. L. Kwon, H.-B. Park, S.-u. Y. Lee, J.-i. Y. Kim, J. Sung, J. M. Kim, K. S. Song, K.-H. Kim, *Transl. Oncol.* **2016**, *9*, 79.
- [20] M. Ducker, V. Millar, D. Ebner, F. G. Szele, *Stem Cell Rep.* **2020**, *15*, 789.
- [21] E. T. Costa, A. A. Camargo, *Methods Mol. Biol.* **2018**, *1731*, 155.
- [22] M. Vinci, C. Box, S. A. Eccles, *JoVE* **2015**, *99*, e52686.
- [23] K. M. Charoen, B. Fallica, Y. L. Colson, M. H. Zaman, M. W. Grinstaff, *Biomaterials* **2014**, *35*, 2264.

- [24] J. Lecomte, A. Masset, S. Blacher, L. Maertens, A. Gothot, M. Delgaudine, F. Bruyère, O. Carnet, J. Paupert, M. Illemann, J.-M. Foidart, I. K. Lund, G. Høyer-Hansen, A. Noel, *Neoplasia* **2012**, *14*, 943.
- [25] J. Ko, J. Ahn, S. Kim, Y. Lee, J. Lee, D. Park, N. L. Jeon, *Lab Chip* **2019**, *19*, 2822.
- [26] J. Guyon, L. Andrique, N. Pujol, G. V. Røslund, G. Recher, A. Bikfalvi, T. Daubon, *J. Vis. Exp.* **2020**, *158*, e60998.
- [27] J.-B. Guy, S. Espenel, A. Vallard, P. Battiston-Montagne, A.-S. Wozny, D. Ardail, G. Alphonse, C. Rancoule, C. Rodriguez-Lafrasse, N. Magne, *J. Vis. Exp.* **2017**, *27*, e56337.
- [28] S. Richbart, J. Merritt, E. Moles, K. Brown, A. Adeluola, P. Finch, J. Hess, M. Tirona, S. Miles, M. Valentovic, P. Dasgupta, *Bio-Protoc.* **2022**, *12*, e4320.
- [29] T. Jiang, J. Munguia-Lopez, S. Flores-Torres, J. Grant, S. Vijayakumar, A. De Leon-Rodriguez, J. M. Kinsella, *J. Vis. Exp.* **2018**, *137*, e57826.
- [30] L. De Moor, S. Fernandez, C. Vercruyssen, L. Tytgat, M. Asadian, N. De Geyter, S. Van Vlierberghe, P. Dubruel, H. Declercq, *Front. Bioeng. Biotechnol.* **2020**, <https://doi.org/10.3389/fbioe.2020.00484>.
- [31] J. M. Lee, D. a Y. Park, L. Yang, E.-J. Kim, C. D. Ahrberg, K. i-B. Lee, B. G. Chung, *Sci. Rep.* **2018**, *8*, 17145.
- [32] J. M. Ayuso, R. Monge, A. Martínez-González, M. Virumbrales-Muñoz, G. A. Llamazares, J. Berganzo, A. Hernández-Laín, J. Santolaria, M. Doblaré, C. Hubert, J. N. Rich, P. Sánchez-Gómez, V. M. Pérez-García, I. Ochoa, L. J. Fernández, *Neuro. Oncol.* **2017**, *19*, 503.
- [33] M. Anguiano, C. Castilla, M. Maska, C. Ederra, R. Peláez, X. Morales, G. Muñoz-Arrieta, M. Mujika, M. Kozubek, A. Muñoz-Barrutia, A. Rouzaut, S. Arana, J. M. Garcia-Aznar, C. Ortiz-De-Solorzano, *PLoS One* **2017**, *12*, e0171417.
- [34] M. Z. I. Mollah, H. M. Zahid, Z. Mahal, M. R. I. Rashed, I. Faruque, *Front. Mol. Biosci.* **2018**, *8*, 719972.
- [35] P. Friedl, K. Wolf, *Nat. Rev. Cancer* **2003**, *3*, 362.
- [36] P. Friedl, S. Alexander, *Cell* **2011**, *147*, 992.
- [37] S. Van Helvert, C. Storm, P. Friedl, *Nat. Cell Biol.* **2018**, *20*, 8.
- [38] P. Friedl, K. Wolf, *J. Cell Biol.* **2010**, *188*, 11.
- [39] A. J. Holder, N. Badii, K. Hawkins, C. Wright, P. R. Williams, D. J. Curtis, *Soft Matter* **2018**, *14*, 574.
- [40] Y. a-L. i Yang, S. Motte, L. J. Kaufman, *Biomaterials* **2010**, *31*, 5678.
- [41] Y. a-L. i Yang, L. J. Kaufman, *Biophys. J.* **2009**, *96*, 1566.
- [42] R. C. Arevalo, J. S. Urbach, D. L. Blair, *Biophys. J.* **2010**, *99*, L65.
- [43] I. K. Piechocka, A. S. G. Van Oosten, R. G. M. Breuls, G. H. Koenderink, *Biomacromolecules* **2011**, *12*, 2797.
- [44] I. Argatov, A. Iantchenko, V. Kocherbitov, *Continuum Mech. Thermo-dyn.* **2017**, *29*, 1375.
- [45] J. Iturri, J. Toca-Herrera, *Polymers* **2017**, *9*, 383.
- [46] C. B. Raub, V. Suresh, T. Krasieva, J. Lyubovitsky, J. D. Mih, A. J. Putnam, B. J. Tromberg, S. C. George, *Biophys. J.* **2007**, *92*, 2212.
- [47] M. Achilli, D. Mantovani, *Polymers* **2010**, *2*, 664.
- [48] Y. a-L. i Yang, L. M. Leone, L. J. Kaufman, *Biophys. J.* **2009**, *97*, 2051.
- [49] E. E. Antoine, P. P. Vlachos, M. N. Rylander, *Tissue Eng., Part B* **2014**, *20*, 683.
- [50] T. Ushiki, *Arch. Histol. Cytol.* **2002**, *65*, 109.
- [51] C. B. Raub, J. Unruh, V. Suresh, T. Krasieva, T. Lindmo, E. Gratton, B. J. Tromberg, S. C. George, *Biophys. J.* **2008**, *94*, 2361.
- [52] R. Pamplona, S. González-Lana, P. Romero, I. Ochoa, R. Martín-Rapún, C. Sánchez-Somolinos, *ACS Appl. Polym. Mater.* **2023**, *5*, 1487.
- [53] T. Ushiki, C. Ide, *Arch. Histol. Jpn.* **1986**, *49*, 553.
- [54] J. Xie, M. Bao, S. M. C. Bruekers, W. T. S. Huck, *ACS Appl. Mater. Interfaces* **2017**, *9*, 19630.
- [55] S. Meehan, A. S. Nain, *Biophys. J.* **2014**, *107*, 2604.
- [56] C.-M. Lo, H.-B. Wang, M. Dembo, Y.-L. Wang, *Biophys. J.* **2000**, *79*, 144.
- [57] B.-H. Mao, M. T. K. Nguyen, M.-J. Tang, R. D. Kamm, T.-Y. Tu, *Biofabrication* **2022**.
- [58] I. Pajic-Lijakovic, M. Milivojevic, A. G. Clark, *Front. Cell Dev. Biol.* **2022**, <https://doi.org/10.3389/fcell.2022.901026>.
- [59] A. Mukherjee, B. Behkam, A. S. Nain, *iScience* **2019**, *19*, 905.
- [60] C. M. Murphy, M. G. Haugh, F. J. O'Brien, *Biomaterials* **2010**, *31*, 461.
- [61] W. Han, S. Chen, W. Yuan, Q. Fan, J. Tian, X. Wang, L. Chen, X. Zhang, W. Wei, R. Liu, J. Qu, Y. Jiao, R. H. Austin, L. Liu, *Proc. Natl. Acad. Sci. USA* **2016**, *113*, 11208.
- [62] H. E. Balcioglu, B. Van De Water, E. H. J. Danen, *Sci. Rep.* **2016**, *6*, 22580.
- [63] J. L. Hutter, J. Bechhoefer, *Rev. Sci. Instrum.* **1993**, *64*, 1868.
- [64] D. Lacalle, H. A. Castro-Abril, T. Randelovic, C. Domínguez, J. Heras, E. Mata, G. Mata, Y. Méndez, V. Pascual, I. Ochoa, *Comput. Methods Programs Biomed.* **2021**, *200*, 105837.
- [65] R. Core Team, *R: A Language and Environment for Statistical Computing*, R Foundation for Statistical Computing, Vienna, Austria **2013**.
- [66] J. Pinheiro, D. Bates, *Mixed-Effects Models in S and S-PLUS*, Springer, New York **2000**.
- [67] J. Pinheiro, D. Bates, R Core Team, nlme: Linear and Nonlinear Mixed Effects Models. **2022**, <https://cran.r-project.org/web/packages/nlme/nlme.pdf> (accessed: June 2023).
- [68] K. Oberauer, *Psychol. Sci.* **2022**, *33*, 648.